REPORT DOCUMENTATION PAGE

Form Approved OMB NO. 0704-0188

1. REPORT DATE (DD-MM-YYYY)	2. REPORT TYPE	3. DATES COVERED (From - To)
24-02-2016	Final Report	17-Sep-2009 - 16-Sep-2015

4. TITLE AND SUBTITLE
Final Report: Design of adaptive load mitigating materials using nonlinear stress wave tailoring

5a. CONTRACT NUMBER
W911NF-09-1-0436

5b. GRANT NUMBER

5c. PROGRAM ELEMENT NUMBER
611103

6. AUTHORS
John Lambros, Chiara Daraio, Philippe Geubelle, Waltraud Kriven, Daniel Tortorelli, Alexander Vakakis

5d. PROJECT NUMBER

5e. TASK NUMBER

5f. WORK UNIT NUMBER

7. PERFORMING ORGANIZATION NAMES AND ADDRESSES
University of Illinois - Urbana
1901 S. First Street, Suite A
Champaign, IL 61820 -7406

8. PERFORMING ORGANIZATION REPORT NUMBER

9. SPONSORING/MONITORING AGENCY NAME(S) AND ADDRESS (ES)
U.S. Army Research Office
P.O. Box 12211
Research Triangle Park, NC 27709-2211

10. SPONSOR/MONITOR'S ACRONYM(S)
ARO

11. SPONSOR/MONITOR'S REPORT NUMBER(S)
56150-MS-MUR.84

12. DISTRIBUTION AVAILIBILITY STATEMENT
Approved for Public Release; Distribution Unlimited

13. SUPPLEMENTARY NOTES
The views, opinions and/or findings contained in this report are those of the author(s) and should not contrued as an official Department of the Army position, policy or decision, unless so designated by other documentation.

14. ABSTRACT
This six-year effort focused on (i) a fundamental understanding of wave propagation of solitary and solitary-like pulses in one- two- and three-dimensional (1D, 2D and 3D) ordered granular media, and (ii) material design, based on these findings, of novel materials with unprecedented impact response properties. Modeling and experimental efforts on wave propagation in 1D, 2D and 3D granular structures were conducted. These were focused on analyzing the dynamic response of granular materials over a range of loading conditions, evaluating scaling laws for force attenuation and energy dissipation, and design using a robust simulation framework optimized granular

15. SUBJECT TERMS
Wave mitigation, granular media, solitary wave, contact, plasticity, impact, material design, optimization

16. SECURITY CLASSIFICATION OF:			17. LIMITATION OF ABSTRACT	15. NUMBER OF PAGES	19a. NAME OF RESPONSIBLE PERSON
a. REPORT	b. ABSTRACT	c. THIS PAGE			John Lambros
UU	UU	UU	UU		19b. TELEPHONE NUMBER 217-333-2242

Standard Form 298 (Rev 8/98)
Prescribed by ANSI Std. Z39.18

Report Title

Final Report: Design of adaptive load mitigating materials using nonlinear stress wave tailoring

ABSTRACT

This six-year effort focused on (i) a fundamental understanding of wave propagation of solitary and solitary-like pulses in one- two- and three-dimensional (1D, 2D and 3D) ordered granular media, and (ii) material design, based on these findings, of novel materials with unprecedented impact response properties. Modeling and experimental efforts on wave propagation in 1D, 2D and 3D granular structures were conducted. These were focused on analyzing the dynamic response of granular materials over a range of loading conditions, evaluating scaling laws for force attenuation and energy dissipation, and design using a robust simulation framework optimized granular structures for specific wave management tasks. Novel physical phenomena such as new nonlinear normal modes in dimers, pass bands, stop bands, and breathers in coupled quasi-1D granular chains embedded in an elastic matrix, lateral energy partition in weakly coupled chains, wave motion control through confinement, etc. were discovered. The material design efforts mainly focused on 1D and 2D geometries involving either granular distributions with spatially optimized granule positions for specific wave mitigation or wave deflection applications, and on rank laminate materials forming a “continuum” specifically designed for wave tailoring. This report provides a summary of both novel physical phenomena and material design performed.

Enter List of papers submitted or published that acknowledge ARO support from the start of the project to the date of this printing. List the papers, including journal references, in the following categories:

(a) Papers published in peer-reviewed journals (N/A for none)

Received		Paper
02/24/2016	76	Raj Kumar Pal, Jeremy Morton, Erheng Wang, John Lambros, Philippe H. Geubelle. Impact Response of Elasto-Plastic Granular Chains Containing an Intruder Particle, Journal of Applied Mechanics, (11 2014): 0. doi: 10.1115/1.4028959
02/24/2016	75	Raj Kumar Pal, Philippe H. Geubelle. Wave tailoring by precompression in confined granular systems, Physical Review E, (10 2014): 0. doi: 10.1103/PhysRevE.90.042204
02/24/2016	74	Mohith Manjunath, Amnaya P. Awasthi, Philippe H. Geubelle. Family of plane solitary waves in dimer granular crystals, Physical Review E, (09 2014): 0. doi: 10.1103/PhysRevE.90.032209
02/24/2016	73	Erheng Wang, Mohith Manjunath, Amnaya P. Awasthi, Raj Kumar Pal, Philippe H. Geubelle, John Lambros. High-amplitude elastic solitary wave propagation in 1-D granular chains with preconditioned beads: Experiments and theoretical analysis, Journal of the Mechanics and Physics of Solids, (12 2014): 0. doi: 10.1016/j.jmps.2014.08.002
02/24/2016	72	E. Kim, R. Chaunsali, H. Xu, J. Jaworski, J. Yang, P. G. Kevrekidis, A. F. Vakakis. Nonlinear low-to-high-frequency energy cascades in diatomic granular crystals, Physical Review E, (12 2015): 0. doi: 10.1103/PhysRevE.92.062201
02/24/2016	71	M. A. Hasan, L. Pichler, Y. Starosvetsky, D. M. McFarland, A. F. Vakakis. Effects of uncertainties on pulse attenuation in dimer granular chains with and without pre-compression, Continuum Mechanics and Thermodynamics, (10 2014): 0. doi: 10.1007/s00161-014-0389-y
02/24/2016	70	M. Arif Hasan, Alexander F. Vakakis, D. Michael McFarland. Nonlinear localization, passive wave arrest and traveling breathers in two-dimensional granular networks with discontinuous lateral boundary conditions, Wave Motion, (01 2016): 0. doi: 10.1016/j.wavemoti.2015.10.001
02/24/2016	80	P.B. Nakshatrala, D.A. Tortorelli. Topology optimization for effective energy propagation in rate-independent elastoplastic material systems, Computer Methods in Applied Mechanics and Engineering, (10 2015): 0. doi: 10.1016/j.cma.2015.05.004
02/24/2016	83	M. Arif Hasan, Shinhu Cho, Kevin Remick, Alexander F. Vakakis, D. Michael McFarland, Waltraud M. Kriven. Experimental study of nonlinear acoustic bands and propagating breathers in ordered granular media embedded in matrix, Granular Matter, (12 2014): 0. doi: 10.1007/s10035-014-0536-y
02/24/2016	82	Christian J. Espinoza Santos, Arif Z. Nelson, Elena Mendoza, Randy H. Ewoldt, Waltraud M. Kriven. Design and fabrication of ceramic beads by the vibration method, Journal of the European Ceramic Society, (11 2015): 0. doi: 10.1016/j.jeurceramsoc.2015.05.018
02/24/2016	79	Pathikumar Sellappan, Erheng Wang, Christian J. Espinoza Santos, Tommy On, John Lambros, Waltraud M. Kriven. Wave propagation through alumina-porous alumina laminates, Journal of the European Ceramic Society, (01 2015): 0. doi: 10.1016/j.jeurceramsoc.2014.08.013
02/24/2016	78	Tommy On, Erheng Wang, John Lambros. Plastic waves in one-dimensional heterogeneous granular chains under impact loading: Single intruders and dimer chains, International Journal of Solids and Structures, (06 2015): 0. doi: 10.1016/j.ijsolstr.2015.02.006

02/24/2016 77 Amnaya Awasthi, Ziyi Wang, Natalie Broadhurst, Philippe Geubelle. Impact response of granular layers, Granular Matter, (01 2015): 0. doi: 10.1007/s10035-015-0547-3

09/07/2014 41 A. Leonard, C. Chong, P. G. Kevrekidis, C. Daraio. Traveling waves in 2D hexagonal granular crystal lattices, Granular Matter, (4 2014): 0. doi: 10.1007/s10035-014-0487-3

09/07/2014 53 Guillaume F Nataf, Pedro O Castillo-Villa, Pathikumar Sellappan, Waltraud M Kriven, Eduard Vives, Antoni Planes, Ekhard K H Salje. Predicting failure: acoustic emission of berlinite under compression, Journal of Physics: Condensed Matter, (07 2014): 0. doi: 10.1088/0953-8984/26/27/275401

09/07/2014 52 Kevin C. Seymour, Waltraud M. Kriven, L. Pinckney. Synthesis and Thermal Expansion of ?-Eucryptite Powders Produced by the Inorganic-Organic Steric Entrapment Method, Journal of the American Ceramic Society, (07 2014): 0. doi: 10.1111/jace.13102

09/07/2014 51 Christian J. Espinoza Santos, Teng-Sing Wei, Bumrae Cho, Waltraud M. Kriven, L. Gauckler. A Forming Technique to Produce Spherical Ceramic Beads Using Sodium Alginate as a Precursor Binder Phase, Journal of the American Ceramic Society, (11 2013): 0. doi: 10.1111/jace.12584

09/07/2014 50 Amnaya P. Awasthi, Kyle J. Smith, Philippe H. Geubelle, John Lambros. Propagation of solitary waves in 2D granular media: A numerical study, Mechanics of Materials, (11 2012): 0. doi: 10.1016/j.mechmat.2012.07.005

09/07/2014 49 Raj Kumar Pal, Amnaya P. Awasthi, Philippe H. Geubelle. Wave propagation in elasto-plastic granular systems, Granular Matter, (10 2013): 0. doi: 10.1007/s10035-013-0449-1

09/07/2014 48 Mohith Manjunath, Amnaya P. Awasthi, Philippe H. Geubelle. Wave propagation in 2D random granular media, Physica D: Nonlinear Phenomena, (1 2014): 0. doi: 10.1016/j.physd.2013.10.004

09/07/2014 47 Mohith Manjunath, Amnaya P. Awasthi, Philippe H. Geubelle. Plane wave propagation in 2D and 3D monodisperse periodic granular media, Granular Matter, (1 2014): 0. doi: 10.1007/s10035-013-0475-z

09/07/2014 46 Raj Kumar Pal, Amnaya P. Awasthi, Philippe H. Geubelle. Characterization of wave propagation in elastic and elastoplastic granular chains, Physical Review E, (1 2014): 0. doi: 10.1103/PhysRevE.89.012204

09/07/2014 45 Philippe H. Geubelle, Raj Kumar Pal. Impact response of elasto-plastic granular and continuum media: A comparative study, Mechanics of Materials, (06 2014): 0. doi: 10.1016/j.mechmat.2014.02.006

09/07/2014 44 Joseph Lydon, K. R. Jayaprakash, Duc Ngo, Yuli Starosvetsky, Alexander F. Vakakis, Chiara Daraio. Frequency bands of strongly nonlinear homogeneous granular systems, Physical Review E, (7 2013): 0. doi: 10.1103/PhysRevE.88.012206

09/07/2014 43 Miguel Molerón, Andrea Leonard, Chiara Daraio. Solitary waves in a chain of repelling magnets, Journal of Applied Physics, (05 2014): 0. doi: 10.1063/1.4872252

09/07/2014 42 Devvrath Khatri, Stephane Griffiths, Duc Ngo, Chiara Daraio. Highly nonlinear solitary waves in chains of hollow spherical particles, Granular Matter, (1 2013): 0. doi: 10.1007/s10035-012-0377-5

09/08/2014 54 E. Wang, T. On, J. Lambros. An Experimental Study of the Dynamic Elasto-Plastic Contact Behavior of Dimer Metallic Granules, Experimental Mechanics, (12 2012): 0. doi: 10.1007/s11340-012-9696-z

09/08/2014 57 Thibaut Detroux, Yuli Starosvetsky, Gaetan Kerschen, Alexander F. Vakakis. Classification of periodic orbits of two-dimensional homogeneous granular crystals with no pre-compression, Nonlinear Dynamics, (1 2014): 0. doi: 10.1007/s11071-013-1160-9

09/08/2014 56 Erheng Wang, Philippe Geubelle, John Lambros. An Experimental Study of the Dynamic Elasto-Plastic Contact Behavior of Metallic Granules,
Journal of Applied Mechanics, (01 2013): 0. doi: 10.1115/1.4007254

09/08/2014 55 Tommy On, Peter A. LaVigne, John Lambros. Development of plastic nonlinear waves in one-dimensional ductile granular chains under impact loading,
Mechanics of Materials, (1 2014): 0. doi: 10.1016/j.mechmat.2013.06.013

09/11/2013 31 Mariana Silva, Daniel A. Tortorelli, Kevin Brittain. Minmax topology optimization,
Structural and Multidisciplinary Optimization, (10 2011): 657. doi: 10.1007/s00158-011-0715-y

09/11/2013 32 Pedro O Castillo-Villa, Jordi Baró, Antoni Planes, Ekhard K H Salje, Pathikumar Sellappan, Waltraud M Kriven, Eduard Vives. Crackling noise during failure of alumina under compression: the effect of porosity,
Journal of Physics: Condensed Matter, (07 2013): 0. doi: 10.1088/0953-8984/25/29/292202

09/11/2013 34 Chau Le, Tyler E. Bruns, Daniel A. Tortorelli. Material microstructure optimization for linear elastodynamic energy wave management,
Journal of the Mechanics and Physics of Solids, (02 2012): 351. doi: 10.1016/j.jmps.2011.09.002

09/11/2013 35 A. Leonard, C. Daraio. Stress Wave Anisotropy in Centered Square Highly Nonlinear Granular Systems,
Physical Review Letters, (05 2012): 214301. doi: 10.1103/PhysRevLett.108.214301

09/11/2013 33 K. R. Jayaprakash, Alexander F. Vakakis, Yuli Starosvetsky. Nonlinear resonances in a general class of granular dimers with no pre-compression,
Granular Matter, (04 2013): 327. doi: 10.1007/s10035-013-0404-1

09/11/2013 36 I. Szelengowicz, M. A. Hasan, Y. Starosvetsky, A. Vakakis, C. Daraio. Energy equipartition in two-dimensional granular systems with spherical intruders,
Physical Review E, (03 2013): 32204. doi: 10.1103/PhysRevE.87.032204

09/11/2013 37 Chiara Daraio, Surajit Sen, Diankang Sun. Nonlinear repulsive force between two solids with axial symmetry,
Physical Review E, (06 2011): 66605. doi: 10.1103/PhysRevE.83.066605

09/11/2013 38 G. Theocharis, N. Boechler, P. G. Kevrekidis, S. Job, Mason A. Porter, C. Daraio. Intrinsic energy localization through discrete gap breathers in one-dimensional diatomic granular crystals,
Physical Review E, (11 2010): 56604. doi: 10.1103/PhysRevE.82.056604

09/11/2013 39 M. Arif Hasan, Shinhu Cho, Kevin Remick, Alexander F. Vakakis, D. Michael McFarland, Waltraud M. Kriven. Primary pulse transmission in coupled steel granular chains embedded in PDMS matrix: Experiment and modeling,
International Journal of Solids and Structures, (10 2013): 3207. doi: 10.1016/j.ijsolstr.2013.05.029

09/11/2013 40 I. Szelengowicz, P. G. Kevrekidis, C. Daraio. Wave propagation in square granular crystals with spherical interstitial intruders,
Physical Review E, (12 2012): 61306. doi: 10.1103/PhysRevE.86.061306

TOTAL: 40

Number of Papers published in peer-reviewed journals:

(b) Papers published in non-peer-reviewed journals (N/A for none)

Received Paper

TOTAL:

Number of Papers published in non peer-reviewed journals:

(c) Presentations

Wei-Hsun Lin Fourth Conference on Particle-Based Methods, September 28-30, 2015 (Particle 2015), Session MoA05: IS-From Discrete Particles to Continuum Models of Granular Mechanics: Elasticity and Wave Propagation II "Study of wave propagation in aqueous close-packed colloidal monolayers using laser based excitation".

Wei-Hsun Lin International Congress on Ultrasonics, May 10-14, 2015 (2 015 ICU Metz), Session: Waves in granular media and structures "Measurement of wave propagating in 1D micro-scale Granular chain".

Waymel R., Salazar de Troya M., Tortorelli D. and Lambros J., "Force Optimization in a 2D Packing of Spheres by Selective Placement of Interstitial Intruders", SEM 2015 Annual Conference & Exposition on Experimental and Applied Mechanics, Costa Mesa, CA, June 8-11, 2015.

Waymel R., Salazar de Troya M., Wang E., Tortorelli D. and Lambros J., "Tailored Elasto-Plastic Wave Redirection in a 2D Granular Array of Spheres by Interstitial Element Control", PACAM XV, Fifteenth Pan-American Congress of Applied Mechanics, Urbana-Champaign, IL, May 18–21, 2015.

Geubelle, P. H., and Manjunath, M. "A new family of solitary plane waves in ordered granular crystals." McMat 2015, Seattle, WA. June 30-July 2, 2015.

Number of Presentations: 5.00

Non Peer-Reviewed Conference Proceeding publications (other than abstracts):

Received Paper

TOTAL:

Number of Non Peer-Reviewed Conference Proceeding publications (other than abstracts):

Peer-Reviewed Conference Proceeding publications (other than abstracts):

Received	Paper

TOTAL:

Number of Peer-Reviewed Conference Proceeding publications (other than abstracts):

(d) Manuscripts

Received	Paper
09/16/2012 10.00	Christian Espinoza-Santos, Tseng-Sing Wei, Bumrae Cho, Waltraud Kriven. A Forming Technique to Produce Spherical Ceramic Beads Using Sodium Alginate as a Precursor Binder Phase, J American Ceramic Society (06 2012)
09/16/2012 11.00	Yuli Starosvetsky, M. Arif Hasan, Alexander F. Vakakis. Nonlinear Pulse Equi-partition in Weakly Coupled Ordered Granular Chains with no Pre-Compression, ASME Journal of Computational and Nonlinear Dynamics (06 2012)
09/16/2012 12.00	R. Potekin, K.R. Jayaprakash, D.M. McFarland, K. Remick, L.A. Bergman, A.F. Vakakis. Experimental Study of Strongly Nonlinear Resonances and Anti-Resonances in Granular Dimer Chains, Experimental Mechanics ( )
09/16/2012 13.00	A. Leonard, C. Daraio, A. Awasthi, P. Geubelle. Effects of weak disorder on stress wave anisotropy in centered square nonlinear granular crystals, Phys Review E (01 2012)
09/16/2012 14.00	Amnaya P. Awasthi, Kyle J. Smith, Philippe H. Geubelle, John Lambros. Propagation of solitary waves in 2D granular media: A numerical study, Mechanics of Materials (01 2012)
09/16/2012 15.00	Erheng Wang, Philippe Geubelle, John Lambros. An Experimental Study of the Dynamic Elasto-Plastic Contact Behavior of Metallic Granules, Journal of Applied Mechanics (01 2012)
09/16/2012 17.00	K. R. Jayaprakash, Alexander F. Vakakis, Yuli Starosvetsky. Solitary waves in a general class of granular dimer chains, Journal of Applied Physics (02 2012)
09/16/2012 18.00	K. R. Jayaprakash, Alexander F. Vakakis, Yuli Starosvetsky. Strongly Nonlinear Traveling Waves in Granular Dimer Chains, Journal of Mechanical Systems and Signal Processing (01 2012)
09/16/2012 19.00	K.R. Jayaprakash, Yuli Starosvetsky, Alexander F. Vakakis, Oleg V. Gendelman. Nonlinear Resonances Leading to Strong Shock Attenuation in Granular Dimer Chains, Journal of Nonlinear Science (01 2012)
09/16/2012 20.00	M.A. Hasan, L. Pichler, Y. Starosvetsky, D.M. McFarland, A.F. Vakakis. Effects of Uncertainties on Pulse Attenuation in Dimer Granular Chains with and without Pre-compression, Journal of Vibration and Acoustics (01 2012)
09/17/2012 22.00	K.R. Jayaprakash, Yuli Starosvetsky, Alexander F. Vakakis, Maxime Peeters, Gaetan Kerschen. Nonlinear normal modes and band zones in granular chains with no pre-compression, Nonlinear Dynamics (03 2010)
09/17/2012 23.00	M.A. Hasan, Y. Starosvetsky, A.F. Vakakis, L.I. Manevitch. onlinear Targeted Energy Transfer and Macroscopic Analogue of the Quantum Landau-Zener Effect in Coupled Granular Chains, Physica D (01 2012)
09/17/2012 24.00	K. R. Jayaprakash, Yuli Starosvetsky, Alexander F. Vakakis. New family of solitary waves in granular dimer chains with no precompression, Physical Review E (10 2012)

09/17/2012 25.00 Yuli Starosvetsky, K. R. Jayaprakash, Alexander F. Vakakis, Gaetan Kerschen, Leonid I. Manevitch. Effective particles and classification of the dynamics of homogeneous granular chains with no precompression,
Physical Review E (09 2011)

09/17/2012 26.00 P. B. Nakshatrala, D. A. Tortorelli, K. B. Nakshatrala. Nonlinear structural design using multiscale topology optimization. Part I: Static formulation,
Computer Methods in Applied Mechanics and Engineering (06 2012)

09/17/2012 27.00 YULI STAROSVETSKY, M. ARIF HASAN, ALEXANDER F. VAKAKIS, LEONID I. MANEVITCH. STRONGLY NONLINEAR BEAT PHENOMENA AND ENERGY EXCHANGES IN WEAKLY COUPLED GRANULAR CHAINS ON ELASTIC FOUNDATIONS,
SIAM J. APPL. MATH (01 2012)

09/17/2012 28.00 Erheng Wang, Tommy On, John Lambros. An Experimental Study of the Dynamic Elasto-Plastic Contact Behavior of Dimer Metallic Granules,
Experimental Mechanics (01 2012)

09/17/2012 29.00 Tommy On, Peter A. LaVigne, John Lambros. Development of plastic nonlinear waves in one-dimensional ductile granular chains under impact loading,
Mechanics of Materials (06 2012)

09/17/2012 30.00 Yuli Starosvetsky, Alexander F. Vakakis. Primary wave transmission in systems of elastic rods with granular interfaces,
Wave Motion (04 2011)

TOTAL: 19

Number of Manuscripts:

Books

Received Book

TOTAL:

Received Book Chapter

TOTAL:

Patents Submitted

Patents Awarded

Awards

John Lambros, 2015, Fellow, American Academy of Mechanics

John Lambros, 2015, UIUC Campus Award for Excellence in Graduate and Professional Teaching

John Lambros, 2015, Frocht Award for Excellence in Mechanics Teaching, Society for Experimental Mechanics

John Lambros, 2010–2015, One of the most cited papers in International Journal of Plasticity (Vol. 26, pp. 93–106)

Graduate Students

NAME	PERCENT_SUPPORTED	Discipline
Robert Waymel	1.00	
We-Hsun Lin	1.00	
Ramathasan Thevamaran	0.50	
M.A. Salazar de Troya	1.00	
Stephanie Ott-Monsivais	0.50	
Raj Pal Kumar	1.00	
Harshit Agrawal	0.25	
Joseph Gonzalez	0.25	
Qi Dang	0.25	
Ahmad Raesi Najafi	0.25	
FTE Equivalent:	**6.00**	
Total Number:	**10**	

Names of Post Doctorates

NAME	PERCENT_SUPPORTED
Andrea Leonard	0.50
FTE Equivalent:	**0.50**
Total Number:	**1**

Names of Faculty Supported

NAME	PERCENT_SUPPORTED	National Academy Member
John Lambros	0.08	
Philippe H. Geubelle	0.08	
Chiara Daraio	0.08	
Alexander Vakakis	0.08	
Daniel Tortorelli	0.08	
Waltraud Kriven	0.08	
FTE Equivalent:	**0.48**	
Total Number:	**6**	

Names of Under Graduate students supported

NAME	PERCENT_SUPPORTED	Discipline
Shi En Kim	0.25	Aeronautics
FTE Equivalent:	**0.25**	
Total Number:	**1**	

Student Metrics

This section only applies to graduating undergraduates supported by this agreement in this reporting period

The number of undergraduates funded by this agreement who graduated during this period: 0.00

The number of undergraduates funded by this agreement who graduated during this period with a degree in science, mathematics, engineering, or technology fields:..... 0.00

The number of undergraduates funded by your agreement who graduated during this period and will continue to pursue a graduate or Ph.D. degree in science, mathematics, engineering, or technology fields:..... 0.00

Number of graduating undergraduates who achieved a 3.5 GPA to 4.0 (4.0 max scale):..... 0.00

Number of graduating undergraduates funded by a DoD funded Center of Excellence grant for Education, Research and Engineering:..... 0.00

The number of undergraduates funded by your agreement who graduated during this period and intend to work for the Department of Defense 0.00

The number of undergraduates funded by your agreement who graduated during this period and will receive scholarships or fellowships for further studies in science, mathematics, engineering or technology fields: 0.00

Names of Personnel receiving masters degrees

NAME
Total Number:

Names of personnel receiving PHDs

NAME
Raj Pal Kumar
Mohith Manjunath
Total Number: **2**

Names of other research staff

NAME	PERCENT_SUPPORTED
Petros Arakelian	0.10
FTE Equivalent:	**0.10**
Total Number:	**1**

Sub Contractors (DD882)

1 a. Caltech 1 b.

00000

Sub Contractor Numbers (c): 2009-03197-01 (A2895)
Patent Clause Number (d-1):
Patent Date (d-2):
Work Description (e): Experimental and numerical study of solitary wave propagation in 1D and 2D ordered ela
Sub Contract Award Date (f-1): 9/17/09 12:00AM
Sub Contract Est Completion Date(f-2): 9/15/15 12:00AM

1 a. Caltech 1 b.

00000

Sub Contractor Numbers (c): 2009-03197-01 (A2895)
Patent Clause Number (d-1):
Patent Date (d-2):
Work Description (e): Experimental and numerical study of solitary wave propagation in 1D and 2D ordered ela
Sub Contract Award Date (f-1): 9/17/09 12:00AM
Sub Contract Est Completion Date(f-2): 9/15/15 12:00AM

Inventions (DD882)

Scientific Progress

See Attachment

Technology Transfer

Nothing to report

Title: Design of adaptive load mitigating materials using nonlinear stress wave tailoring
Contract/Grant number: W911NF-09-1-0436
Principal Investigator: John Lambros
Performing Organization Name(s) and Address(es): University of Illinois
1901 S First Street, Suite A
Champaign, IL 61820-7406

ARO proposal number: 56150-MS-MUR

ABSTRACT

This six-year effort focused on (i) a fundamental understanding of wave propagation of solitary and solitary-like pulses in one- two- and three-dimensional (1D, 2D and 3D) ordered granular media, and (ii) material design, based on these findings, of novel materials with unprecedented impact response properties. Modeling and experimental efforts on wave propagation in 1D, 2D and 3D granular structures were conducted. These were focused on analyzing the dynamic response of granular materials over a range of loading conditions, evaluating scaling laws for force attenuation and energy dissipation, and design using a robust simulation framework optimized granular structures for specific wave management tasks. Novel physical phenomena such as new nonlinear normal modes in dimers, pass bands, stop bands, and breathers in coupled quasi-1D granular chains embedded in an elastic matrix, lateral energy partition in weakly coupled chains, wave motion control through confinement, etc. were discovered. The material design efforts mainly focused on 1D and 2D geometries involving either granular distributions with spatially optimized granule positions for specific wave mitigation or wave deflection applications, and on rank laminate materials forming a "continuum" specifically designed for wave tailoring. This report provides a summary of both novel physical phenomena and material design performed.

INTRODUCTION

This report describes the six-year efforts of this MURI project between the periods of September 2009 and 2015 (3 year base funding, 2 year option funding and 1 year no-cost extension). The overarching goal of the effort was to design novel heterogeneous materials that possess revolutionary stress wave mitigating characteristics. The fundamental premise of the design sought to exploit unique wave propagation properties that are present in granular media. Early studies of wave propagation in granular media, primarily in one-dimensional (1D) chains of elastic spherical beads in contact, had shown the development of different nonlinear wave phenomena than those present in an "equivalent" elastic continuum. For example a nonlinear solitary wave has been know to develop in 1D elastic granular chains (Nesterenko, 1984). Such a nonlinear elastic wave exhibits distinct behavior from continuum elastic stress waves in that it has a fixed compact support (i.e., has a fixed pulse duration/wavelength regardless of loading pulse shape), does not have a fixed speed (it speed is proportional to the sixth power of the amplitude) and consequently has decreasing speed with decreasing amplitude (sonic vacuum) (Nesterenko, 2001). These novel physical effects are a direct result of the way in which force "propagates" or transfers in an elastic granular medium and this is namely by material elements (the spherical granules) which interact through nonlinear contact (Hertzian contact in the elastic case). Stemming from the discovery of such solitary waves in 1D elastic granular media, a number of additional studies showed that unique responses were possible such as filtering (frequency ranges where strong wave energy dissipation occurs), tunability (changing wave speed depending on energy level and pre-compression) and energy trapping (energy confinement in preferential locations) (Spadoni and Daraio, 2010 ; Boechler *et al*., 2011).

To achieve our goal of design novel heterogeneous materials for wave mitigation purposes we needed to both develop a fundamental understanding of a number of unanswered questions in the wave mechanics of granular media, and also develop a framework of material design involving computational material design, material fabrication, and design validation. Thus two distinct types of efforts were studies in this research work: **A.** Fundamental studies for the understanding of wave propagation of solitary and solitary-like pulses in one- two- and three dimensional (1D, 2D and 3D) ordered granular media, and **B.** material system design and validation efforts for achieving systems with novel wave propagation and mitigation characteristics. Each type of work is described briefly in the two sections below. By necessity of keeping this final report as concise as possible only the most fundamental outcomes of each of these concentrations will be discussed here in the final report. The details of each of these aspects have been presented in the annual reports already submitted in the past.

The research team that tackled this task consisted of a diverse pool of talent of graduate and undergraduate students, postdoctoral researchers and faculty. A listing of the faculty participants over the duration of the project and their areas of expertise is given below. A more detailed listing of all personnel involved is given in the last section which deals with possible metrics of assessment of the outcomes of this MURI effort.

- Prof. Chiara Daraio (initially at Aeronautics at Caltech and then at ETH Zurich in Switzerland) worked on performing experiments analysis and simulations of model granular media.
- Prof. Philippe Geubelle (UIUC, Aerospace) is an expert on computational simulations and dealt with the simulation and modeling of 1D, 2D and 3D granular media primarily based on a molecular dynamics framework (by modifying LAMMPS for granular material use).

• Prof. Trudy Kriven (UIUC, Materials Science) is an expert in ceramic and geopolymer fabrication.

• Prof. John Lambros (UIUC, Aerospace) is an expert in experimental mechanics of dynamically loaded materials and structures and primarily performed dynamic experimentation on 1D and 2D granular systems.

• Prof. Dan Tortorelli (UIUC, Mechanical) is an expert on numerical optimization and primarily studied material design optimization to obtain desired material response under dynamic loading..

• Prof. Alex Vakakis (UIUC, Mechanical) is an expert on theoretical non-linear dynamics and performed mainly theoretical solutions of a number of fundamental problems in 1D and 1.5D granular material dynamics.

ORGANIZATION OF FINAL REPORT

This report is presented in two parts. In **Part A** a discussion of the main results of our fundamental studies is presented. As mentioned above, in the interest of brevity only major results are presented. Both details of the techniques used and also intermediate milestone results are not presented here as most have been covered in prior interim year reports. **Part B** presents in a similar fashion our main efforts and results in terms of designing material systems based on our understanding of the granular media.

The **list of topics** below presents the major topics studied and the page number where they are described in order to facilitate searching the document:

Topic **Page #**

PART A – DISCOVERY: FUNDAMENTAL STUDIES

PART B – DEMONSTRATION: MATERIAL DESIGN

PART A – DISCOVERY: FUNDAMENTAL STUDIES

A1. 1D-elastic: Pass bands and stop bands in 1D granular chains

We studied pass and stop bands in uncompressed, homogeneous one-dimensional granular media, and showed that they are tunable with energy. In pass bands these media exhibit strongly nonlinear and discontinuous acoustics. In stop bands the granular media are in states of strong effective compression so their acoustics are linearized. The effects of these energy-tuned acoustic bands on the dynamics of granular media are profound as shown in the plots below. In Figure A1.1a a homogeneous granular chain of 50 beads is harmonically forced with a frequency and amplitude corresponding to a state inside a pass band, so the forced response is spatially extended. In Figure A1.1b, the frequency and amplitude of the harmonic force amount to a response inside a stop band so the forced response is spatially localized. These results can be used for designing ordered granular media as vibration and shock mitigators.

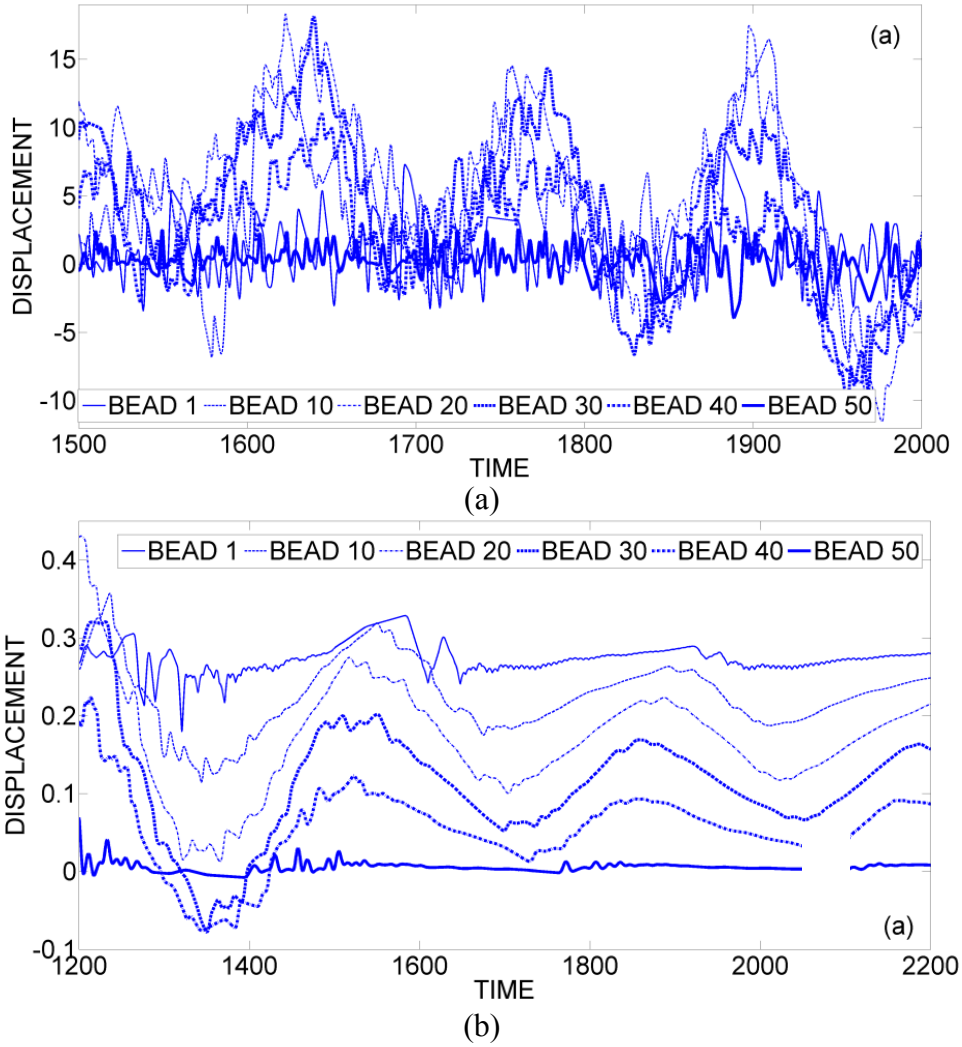

(b)

Figure A1.1: Forced responses of selected beads of a homogeneous granular chain forced by a harmonic displacement excitation of bead 0: Response (a) in the pass band, and (b) in the stop band.

A2. 1D-elastic: Resonances and antiresonances in uncompressed dimer chains – impulsive and harmonic loading

We studied the dynamics of uncompressed dimer chains and proved the existence of countable infinities of resonances (R) and antiresonances (AR) in these systems, depending on the mass ratio between the "heavy" and "light" beads of these chains. Resonances correspond to maximum dispersion of propagating pulses in the dimer and occur when the light bead is set into resonance and vibrates quickly between the two heavy beads, whereas anti-resonances correspond to solitary way propagation, i.e., to unhindered energy transmission through the dimer, in which the light bead and the adjacent heavy beads all move in phase. In Figure A2.1 we present the normalized transmitted force at the right boundary of a dimer (composed of "heavy" beads with normalized mass unity, and "light" beads with normalized mass ε) subject to an impulse of intensity F applied on the left boundary; the normalization of the transmitted force is with respect to the force that would be transmitted in the corresponding homogeneous chain composed only of "heavy" beads. The normalized transmitted force is plotted against the mass ratio ε. We see that we can design the dimer chain so that the transmitted pulse is reduced by as much as 75% compared to the pulse transmitted in the corresponding homogeneous chain.

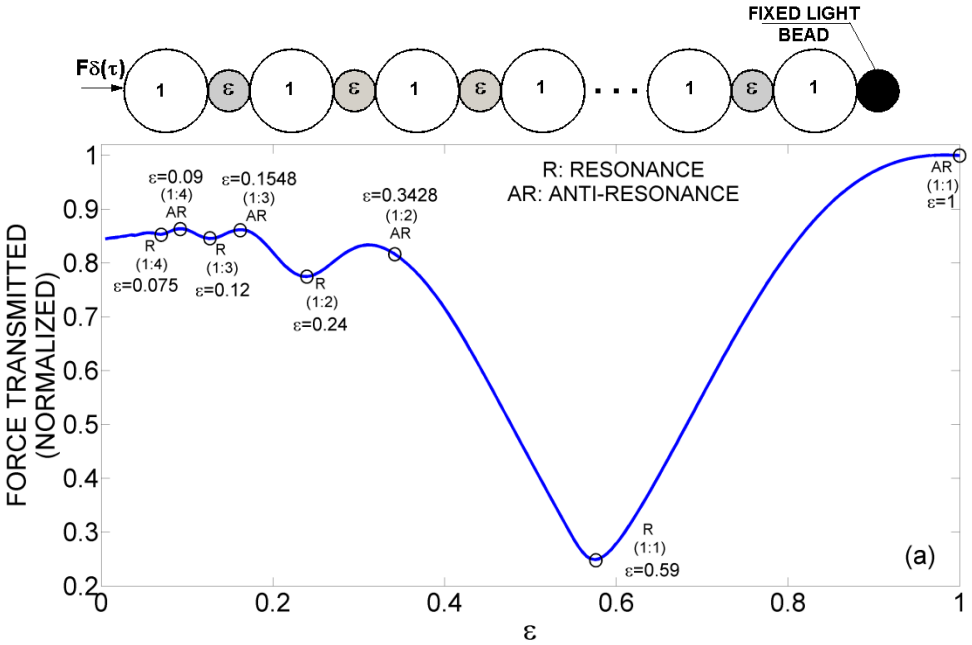

Figure A2.1: Resonances (R) and antiresonances (AR) in the impulsively forced dimer chain.

These theoretical results were also experimentally validated. We used the experimental fixture of Figure A2.2a, and the results are depicted in Figure A2.2b. In this set-up a series of "hanging" beads in a dimer chain was impacted by a striking pendulum bead. In these plots θ represents the angle of the forcing pendulum used to apply the impulse excitation at the left boundary. For the different combinations of values of ε a very good agreement between the experimental measurements and the model is seen.

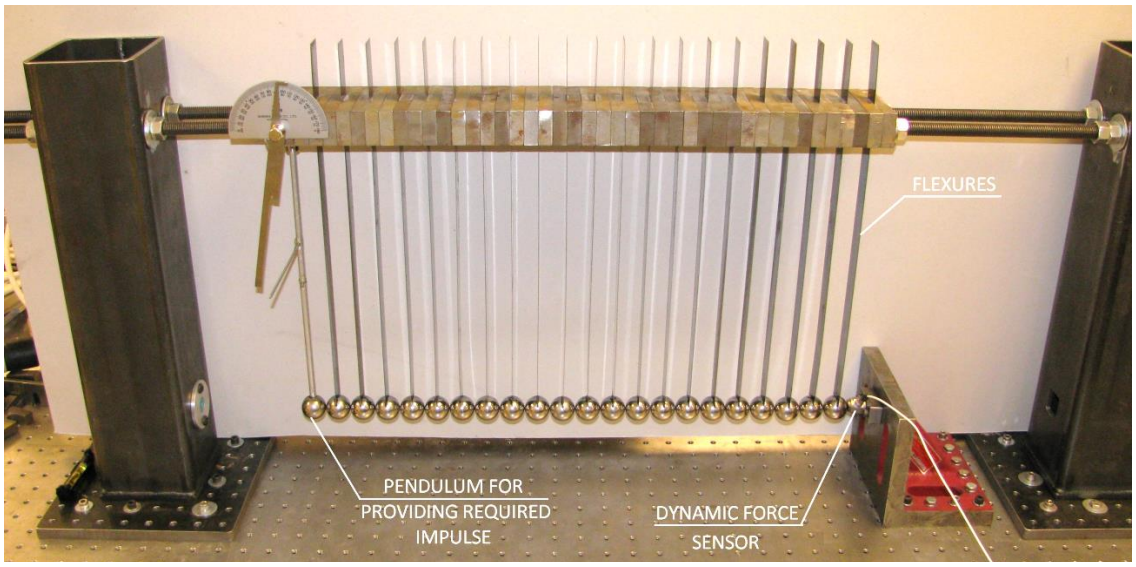

(a)

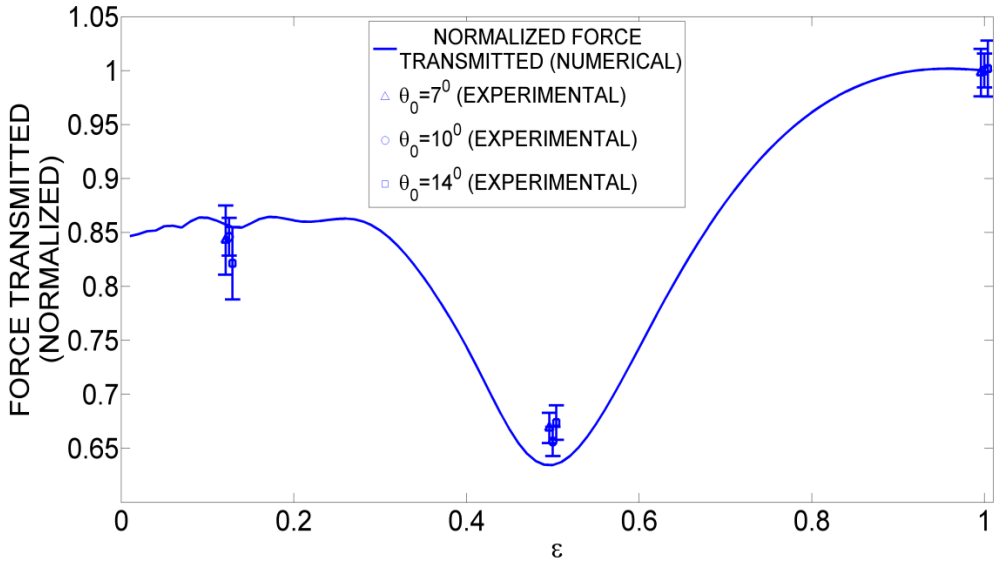

(b)

Figure A2.2: Experimental verification of resonances and antiresonances in the dimer chain.

In addition to the decrease of amplitude in the impulsively generated wave shown above, we also studied forced resonances of finite homogeneous and dimer chains but now with **harmonic displacement excitations** at their left boundaries (see Figure A2.3a). For a chain composed of 21 beads the maximum transmitted steady state force is presented in Figure A2.3b for varying frequency but constant amplitude of excitation. At the peaks (forced resonances) the response of the granular chain is wave-like, whereas at the valleys (forced antiresonaces) is standing wave-like. ***These results contribute to the use of granular media not only as impact protectors but also as vibration isolators.***

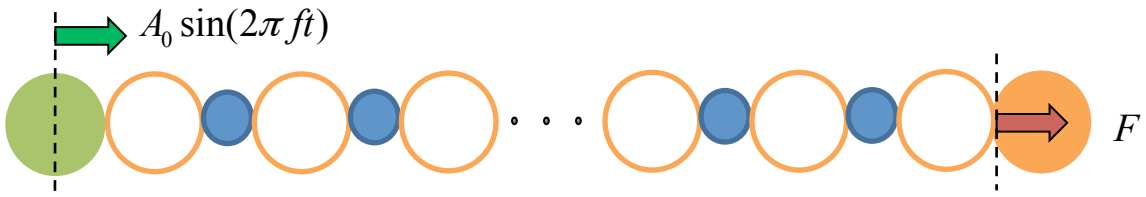

(a)

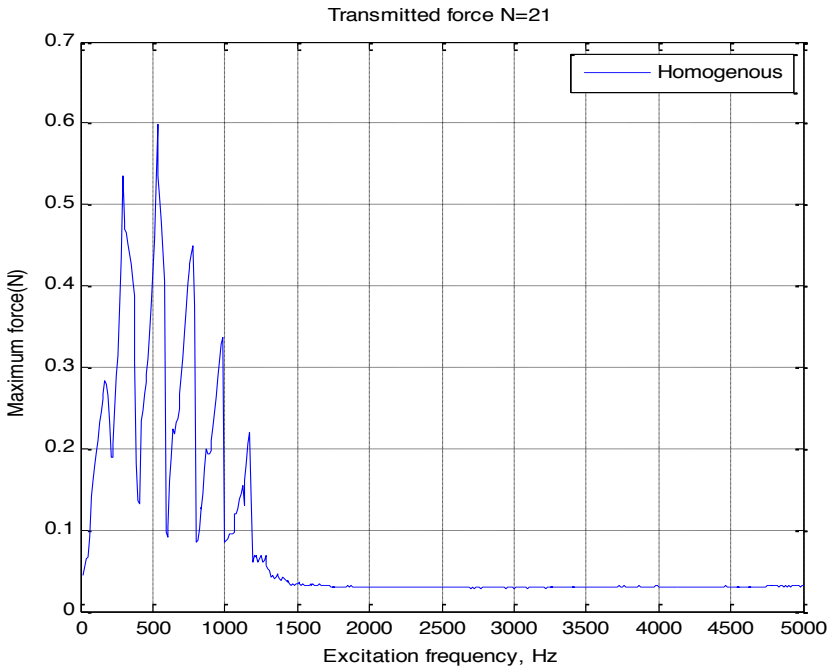

(b)

Figure A2.3: Forced resonances and antiresonances in a harmonically forced finite granular chain.

A3. 1D-elastic: Travelling breathers in granular chains embedded in matrix

We proved the existence of traveling breathers and strong energy exchanges in two-dimensional coupled chains of granular media. In Figure A3.1a we depict a weakly coupled system composed of two homogeneous granular chains, with an impulse excitation applied to the lower chain (designated as "excited" chain), and the upper chain designated as "absorbing" chain. Each chain was supported by a uniform linear elastic foundation. In Figure A3.1b we show the spatiotemporal evolution of the kinetic energy of the beads of this network, where the breather formation is clearly deduced as intense and recurrent energy exchanges between the two networks. Based on these results we were able to ***design the network for passive wave redirection***. This was achieved by linear stratification of the elastic foundation of the excited chain (the same result can be achieved by stratifying the linear coupling between chains) as shown in Figure A3.2a, and inducing the macroscopic analogue of the Landau-Zener quantum tunneling effect in space. This is shown in Figure A3.2b where we see that a pulse initially generated in the excited chain is passively and irreversibly redirected to the absorbing chain, so no recurrent energy exchanges occur in this case. ***This raises the exciting prospect of designing acoustic metamaterials based on granular media with inherent properties for pulse and energy redirection.***

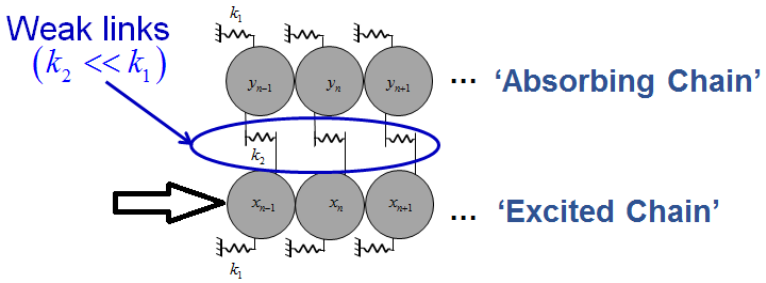

(a)

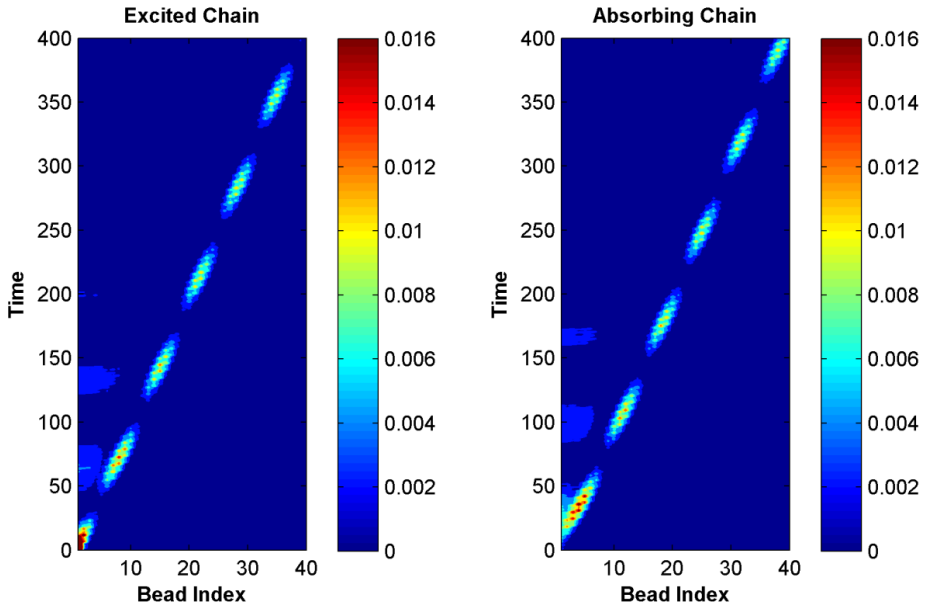

(b)

Figure A3.1: Breather formation in the weakly coupled network of homogeneous granular chains under shock excitation.

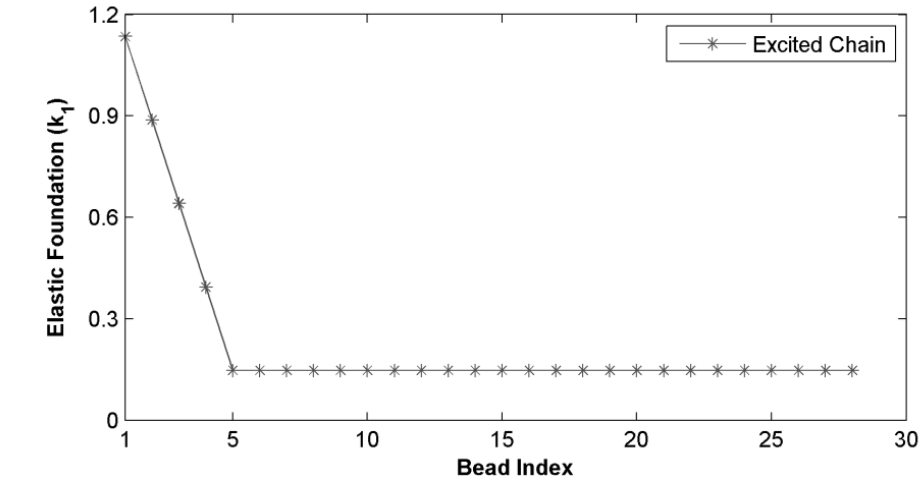

(a)

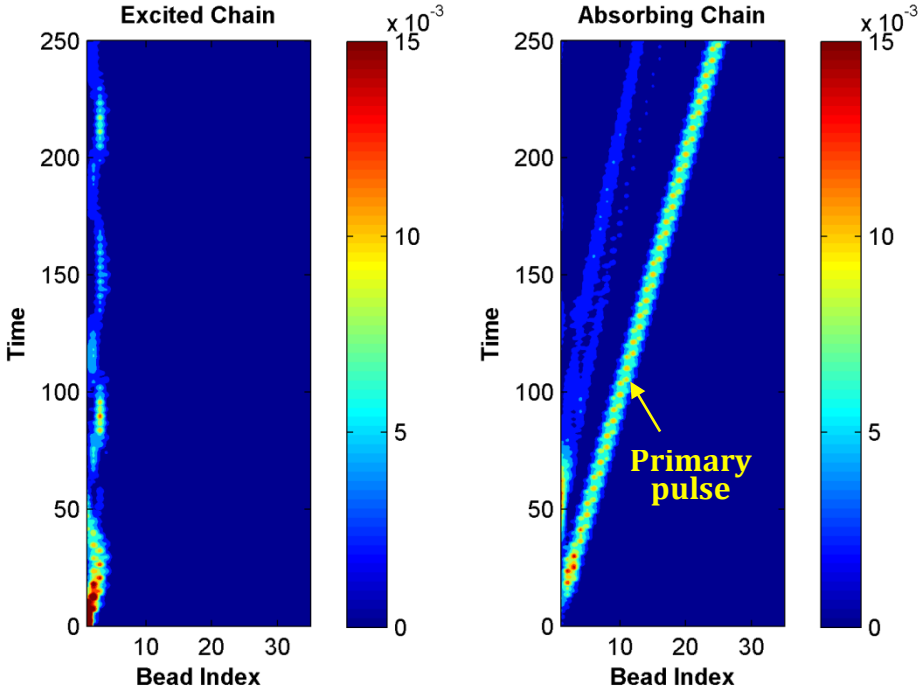

(b)

Figure A3.2: Design for passive pulse and energy redirection in the weakly coupled granular network: (a) Required spatial stratification of the elastic foundation of the excited chain, (b) spatiotemporal kinetic energy evolution showing the passive pulse redirection from the impulsively forced excited chain to the absorbing chain.

A validation of these phenomena was performed based on designed and fabricated ***granular networks embedded in viscoelastic matrix***. These were either single embedded chains (see Figure A3.3a) or coupled embedded chains (see Figure A3.3b). These chains were tested under impulsive and harmonic excitations. In Figure A3.4 we depict the experimental apparatus constructed for testing under impulsive (Figure A3.4a) and harmonic excitations (Figure A3.4b).

A variety of interesting dynamical phenomena have been discovered/validated from these experimental arrangements, including:

• Energy partition: Energy equipartition between coupled chains; that is, energy initially imparted in one of the chains ends up being equipartitioned between the chains of the network;
• Breathers: Forced breathers in single and coupled chains, and intense energy exchanges in coupled chains;
• Filtering: Acoustic filtering properties that are tunable with energy, including low-frequency pass bands and high-frequency pass bands.

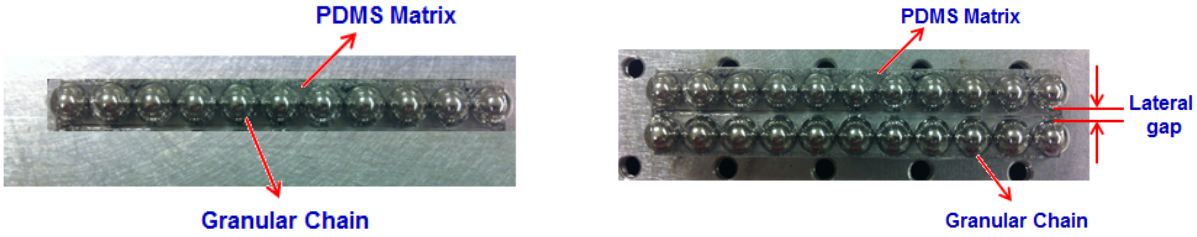

(a) (b)

Figure A3.3: Embedded granular chains in viscoelastic matrix: (a) Single chain, (b) Coupled chains.

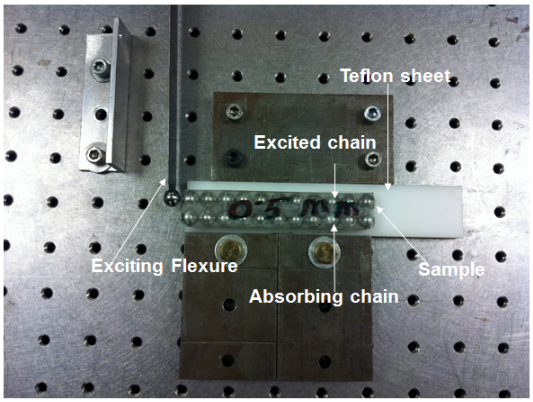

(a)

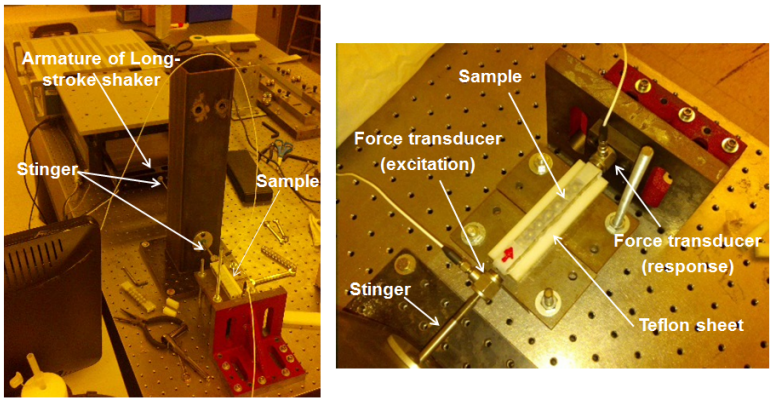

(b)

Figure A3.4: Experimental fixtures for studying the responses of (a) impulsively forced granular media, and (b) harmonically excited granular media.

As an indicative example of the experimental results, in Figure A3.5 we depict experimental traveling breathers in the excited chain of a coupled granular network under harmonic excitation, for three types of viscoelastic matrix. We note that the material properties of the matrix affect the topology of the propagating breather and its frequency and wavenumber content.

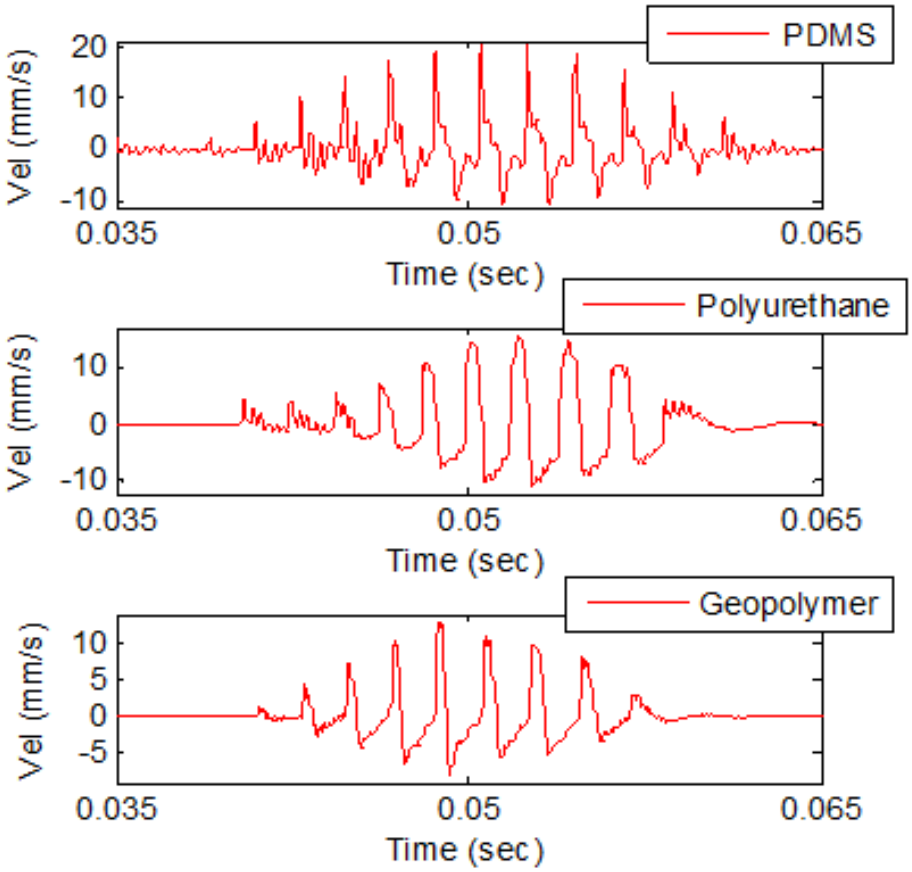

Figure A3.5: Experimental breathers in harmonically forced granular media with three different types of embedding material matrices.

A4. 1D-elastic: Highly nonlinear solitary waves in chains of ellipsoidal or cylindrical beads

We performed experimental tests on chains composed of uniform ellipsoidal particles or cylindrical particles, to study the effect of particle geometry on the stress wave propagation. The experimental setups for chains of ellipsoidal beads or cylindrical beads are presented in Figure A4.1, together with the typical experimental data that we obtained. The experiments showed that the systems of ellipsoidal or cylindrical beads also support the formation and propagation of the highly nonlinear solitary waves. The solitary wave speed – force amplitude scaling obtained experimentally agrees very well with the results obtained from theory and discrete simulations based on Hertzian elliptical contact law, as shown in Figure A4.2. The theory and discrete simulations also predict that the dynamic behavior of the solitary wave (amplitude, speed) depends strongly on the orientation angles between particles in the chain and more detailed researches on this issue are under conducting. This interesting dependence on orientation angle between beads provides another free parameter to employ in tuning the dynamics of the solitary waves propagating in 1-D chain of ellipsoidal or cylindrical beads which cannot be achieved in the chain of spherical beads.

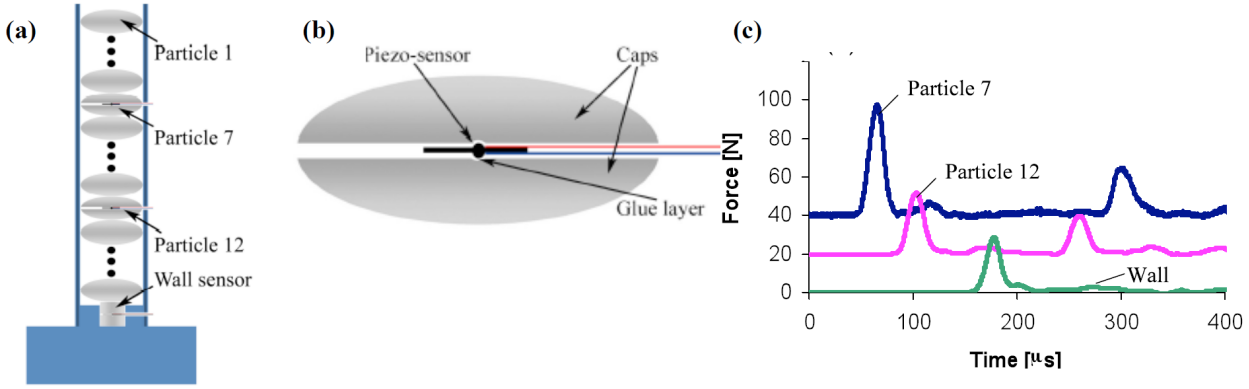

Figure A4.1: (a) Experimental setup of a vertical stacked chain of 20 stainless steel ellipsoidal beads, the orientation angle between two adjacent beads is $\alpha=0°$. Piezoeletric sensors were embedded in particles 7 and 12, as well as at the wall. (b) Schematic diagram representing the assembly of the piezo-gauges embedded in the ellipsoidal particles. (c) Formation of solitary waves excited by impact in a chain of 20 stainless steel ellipsoidal beads. Sensors were at position 7, 12, and at the wall. Impact was generated with 3.787 g striker traveling at 0.75 m/s; the average wave speed was calculated at 525 m/s.

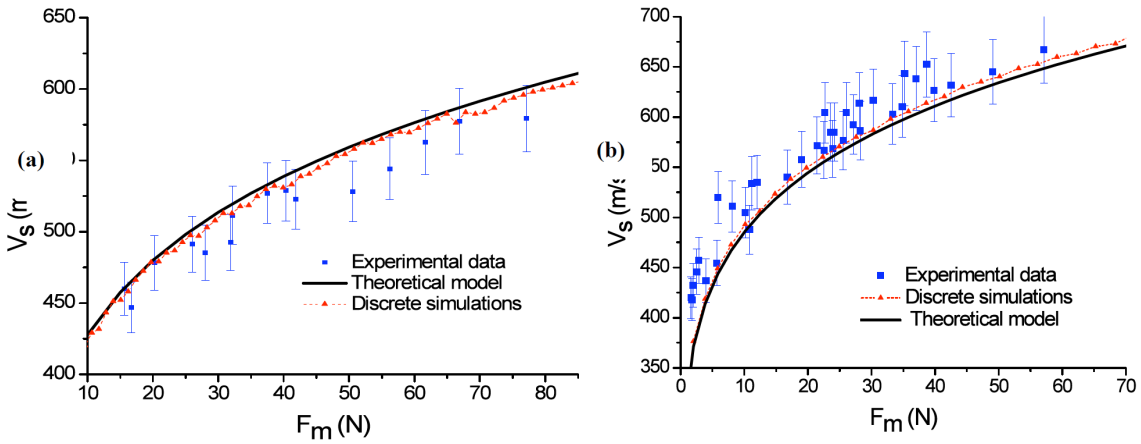

Figure A4.2: Dependence of the wave speed on the maximum contact dynamic force (a) in the chain of ellipsoidal particles, (b) in the chain of cylindrical particles. Experimental values are shown by solid squares. The solid line represents the theoretical prediction based on Hertzian elliptical contact law. The dash line represents the numerical values obtained from discrete simulations.

A5. 1D-elastic: Interaction of highly nonlinear solitary waves with linear elastic media

We studied the interaction of a highly nonlinear solitary wave with an adjacent linear elastic medium (Figure A5.1). The effects of interface dynamics on the temporary localization of incident waves and their decomposition into primary and secondary reflected waves were investigated. Experimental tests were performed to correlate the linear medium geometry, material, and mass with the formation and propagation of the reflected waves. Studying variations of the reflected waves velocity and amplitude, we report on how the propagation of primary and secondary solitary waves responds sensitively to the states of the adjacent linear media. This preliminary study suggests the use of reflected solitary waves in non-destructive evaluation of elastic materials and as a mean to assess mechanical properties of bounding media.

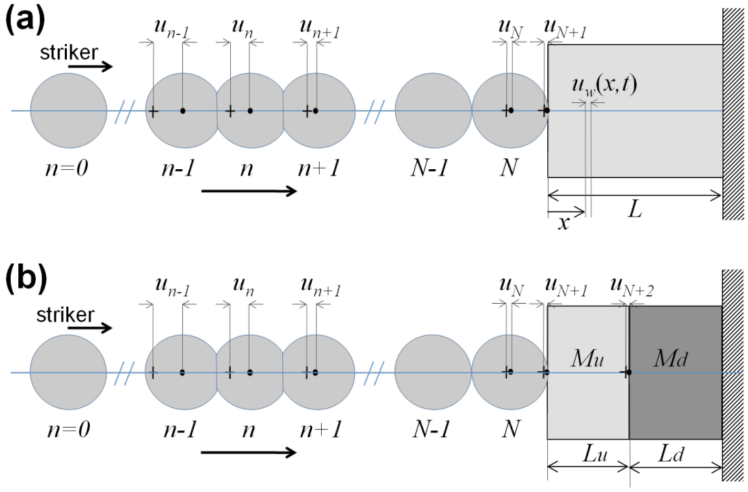

Figure A5.1: Schematic diagram showing the 1D chain of spherical elements in contact with (a) a uniform linear medium and (b) a composite linear medium. The bottom of the linear media is under fixed boundary conditions. All force interactions are restricted under 1D consideration

A6. 1D-elastic: Study of highly nonlinear solitary waves in chains of thin coated spheres

We studied the dynamic response of a chain composed of spherical steel particles coated with a soft polymeric material and showed that these systems support the formation and propagation of highly nonlinear solitary waves. We showed that the dynamic response of chains of coated spheres is governed by a quadratic power law between the contact force, F, and the displacement, δ, instead of the Hertzian, non-integer power of 3/2. This new nonlinear contact interaction changes dramatically the dynamics of the solitary wave propagating in the systems compare to its counterpart in chains of solid spheres, the spatial width of the wave becomes shorter (3.14 particles size instead of 5) and the wave speed (V_s) is relatively slow and its dependence on force amplitude (F_m) is also different ($V_s \sim F_m$ 1/4 instead of $V_s \sim F_m$ 1/6). DP simulations predicted that the dynamic behavior of the solitary wave (amplitude, speed) depends on the thickness of the coating layer Figure A6.1b. This interesting dependence on coating thickness provides another free parameter to employ in tuning the dynamics of the highly nonlinear solitary waves propagating in 1-D chains of coated spheres.

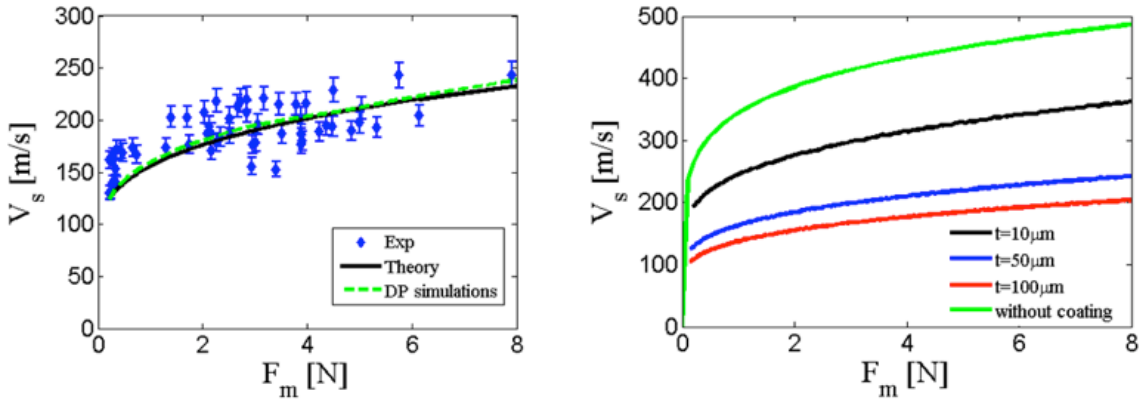

Figure A6.1: (a) Relation of wave speed to force amplitude of solitary wave in the chains of thin-coated spheres. Experimental values are represented by blue dots, theoretical predictions and DP simulations based on thin coating contact law are represented by black and green lines respectively (b) Dependence of wave speed- force amplitude relation on the coating thickness obtained from DP simulations.

A7. 1D-elastic: highly nonlinear solitary waves in chains of hollow spheres

We performed experiments on chains composed of uniform aluminum hollow spheres. The experimental setup is presented in Figure A7.1ab, together with the typical experimental data (Figure A7.1c) that we obtained. We observed the existence of highly nonlinear solitary wave travelling in the system, but the wave properties are different from the highly solitary wave's properties in the chains of solid spheres. The spatial width of the solitary wave in chain of hollow sphere was approximately 8 particles size (larger than 5 beads size), and the wave speed was proportional to force amplitude to power 1/11. FEM studies showed that the contact interaction between thin hollow spheres could be approximated by a power-law type relation ($F=k\delta^n$), in which the exponent n is smaller than the value 3/2 as in the classical Hertzian interaction between solid spheres. The contact stiffness k and the exponent n were also found to be dependent on the shell's thickness of the hollow spheres. The theoretical predictions and DP simulations based on this contact law and FE simulations showed good agreements with the experimental results as shown in Figure A7.1d. The effect of shell thickness on the dynamic response of the system also is presented in Figure A7.1d.

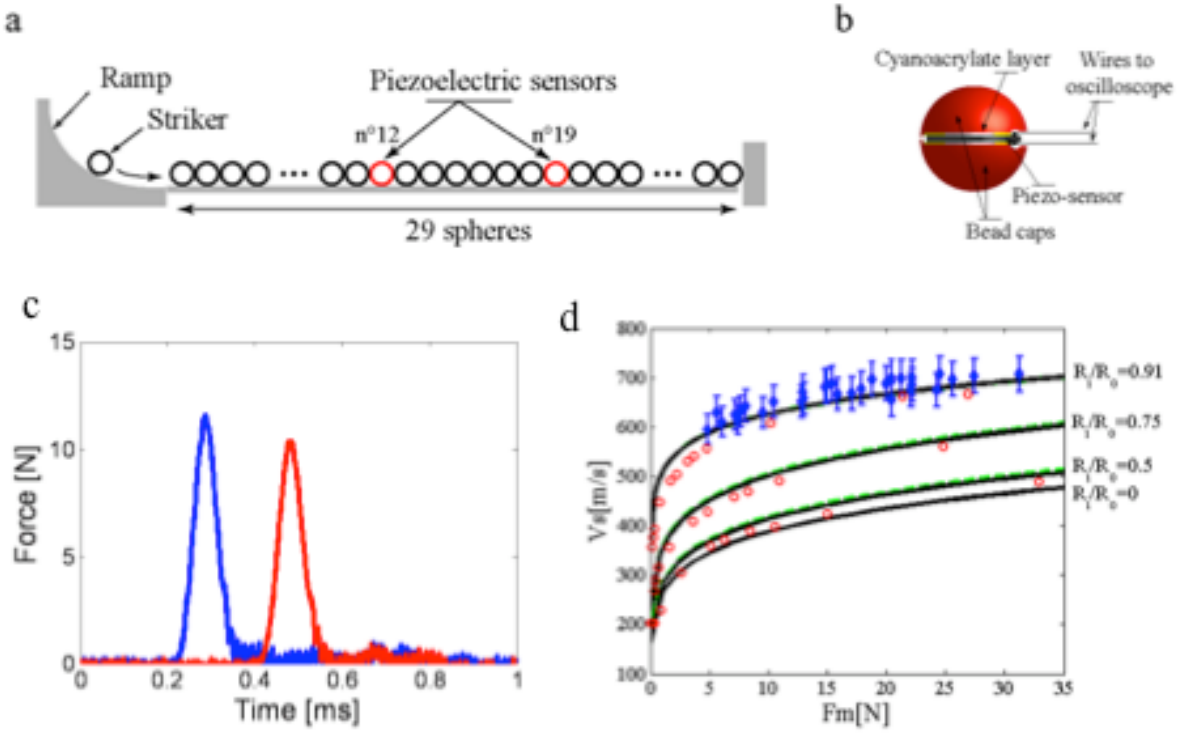

Figure A7.1: (a) Experimental setup of a horizontal chain of 29 hollow aluminum beads. (b) Piezoeletric sensors were embedded in particles 12 and 19. (c) Formation of solitary waves in the chain excited by impact of an identical striker traveling at 0.4 m/s; the average wave speed was calculated at 686 m/s. (d) Relation of wave speed to force amplitude in the chain of hollow spheres for different values of thickness of the hollow spheres. Experimental values are shown by solid (blue) diamonds. The solid (black) lines represent the theoretical predictions. The dash (green) lines represent the numerical values obtained from DP simulations. The red open circles are the results from FE simulations.

A8. 1D-elastic: Granular system with magnetic interaction

We built a one-dimensional granular system with magnetic interactions where the granular elements do not come into direct contact but interact with each other through nonlinear magnetic forces (Figure A8.1). We developed procedures for calibrating the magnetic force and performed digital image correlation (DIC) measurement to determine locations of particles to study the dynamic response of the system.

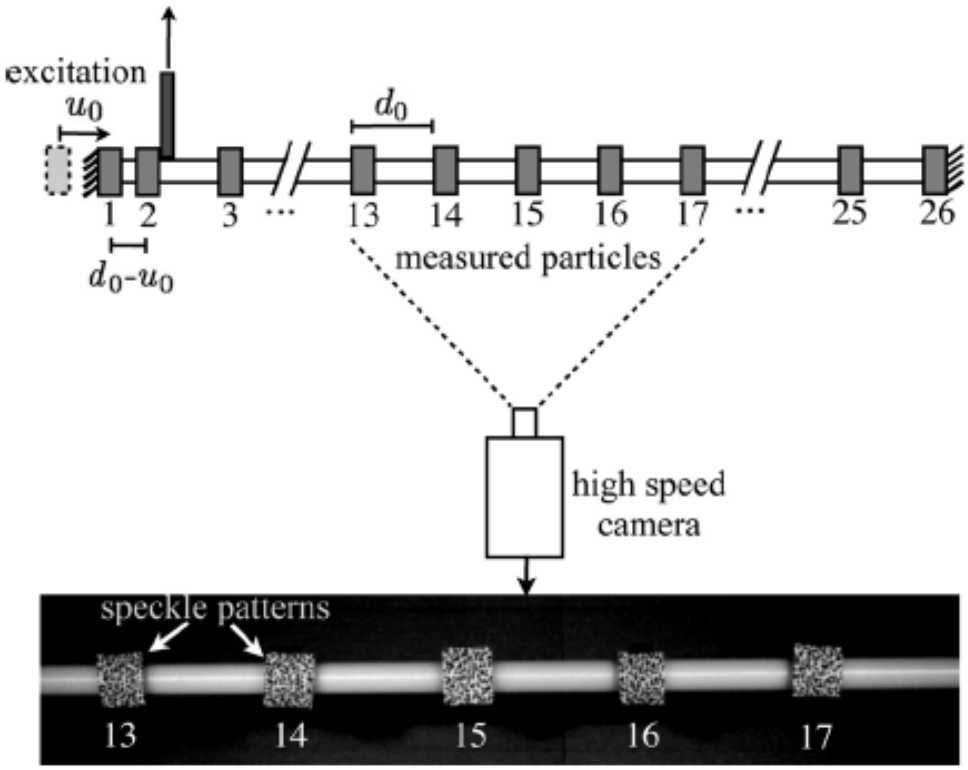

Figure A8.1: Schematics of the magnetic particles experimental setup. The chain is formed by 26 ring magnets placed around a plastic rod. To excite the system, we give an initial displacement to magnet 1. A high-speed camera records the motion of magnets 13 to 17 and DIC is used to extract the displacement and velocity of the particles. The lower picture shows a snapshot of the system at rest.

We investigated the propagation of solitary waves in such a 1D nonlinear lattice of repelling magnets. This system showed an interesting nonlinear dynamic behavior, which support the formation and propagation of solitary waves and it is sensitive to the amplitude of the initial stress excitation. In the low energy regime, the profile of the solitary wave is given by a KdV soliton with a sech2 shape. In the high-energy regime, the wavelength progressively shrunk, with the limiting case reducing into a hat function, with width equal to a single lattice period (atomic scale localization). Such systems could find potential applications in energy mitigation and localization, or in the design of acoustic lenses capable of omitting very narrow pulses. In addition, they can be used to study the fundamental response of nonlinear dynamical systems.

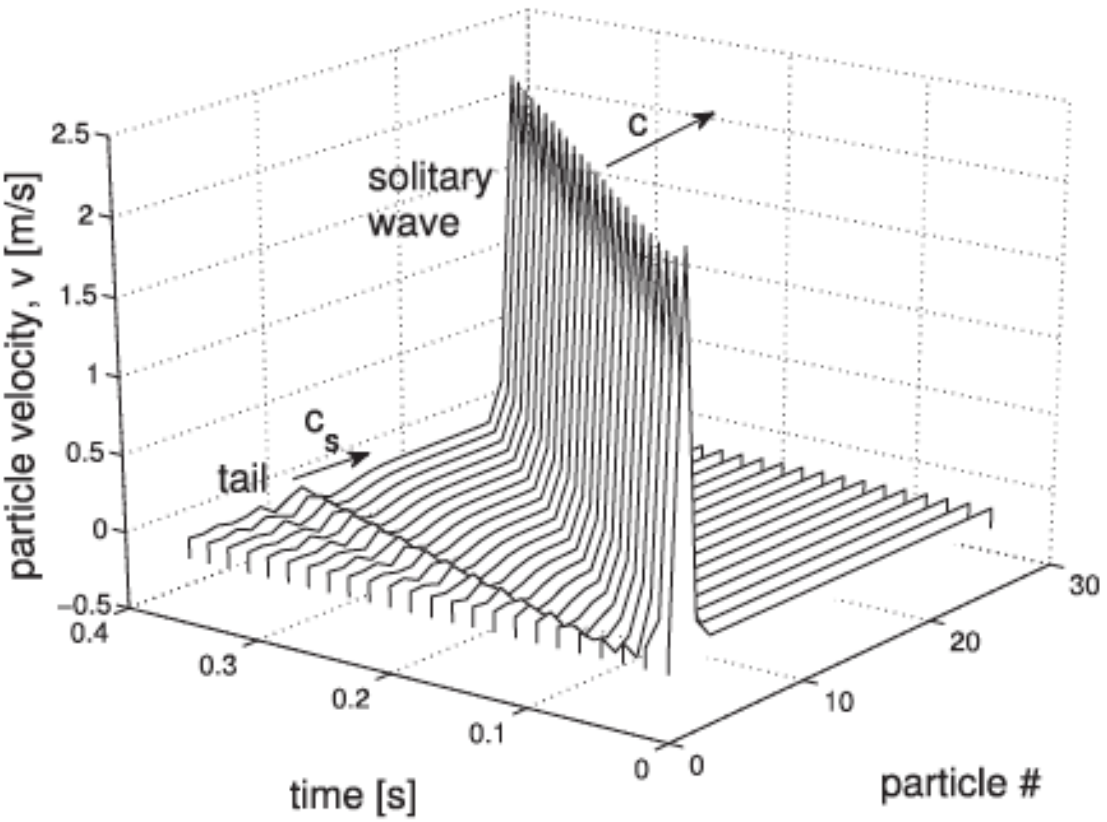

Figure A8.2: Numerical results showing the formation and propagation of a solitary wave in a chain of repelling magnetic particles. The curves show the particle velocity for the particles at different time steps.

A9. 1D-elastic: Nonlinear, locally resonant granular crystals

We studied the acoustic properties of a statically compressed chain of eleven MinM (mass-in-mass) units (Figure A9.1), observing the characteristic band-gap structure due to the presence of local resonators. We observed a nonlinear behavior deriving from the nonlinear contact between the spheres. This nonlinearity resulted in the ability to tune the transmission spectrum and band gap edges of the dispersion relation, by varying the applied static precompression. We also showed that the band gaps can be tuned by variation of the driving excitation amplitudes. Finally, we developed a finite element model of the particles to characterize the vibrational modes of the particles' cavity. The presence of additional modes in the cavity suggested the possibility to design units with multiple resonators.

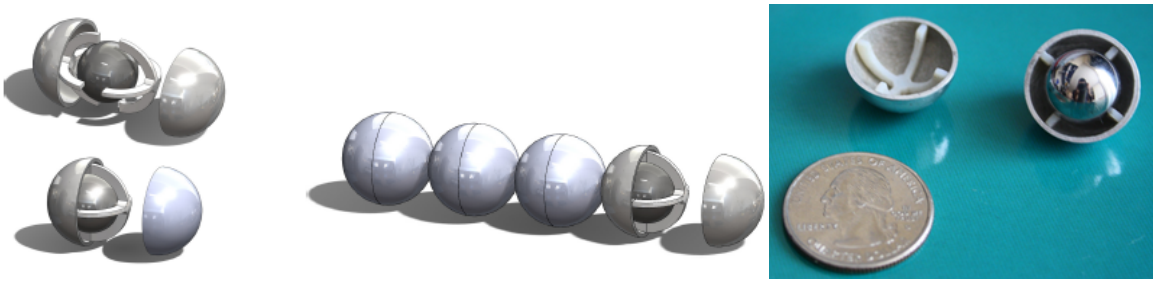

Figure A9.1: Schematic diagram and digital image of the resonant granular particles.

Our study of granular chains with local resonances (Fig. 24) revealed that it is possible to achieve very high vibration mitigation at selected frequencies by attaching each of the beads of a granular chain to a local resonator. We explored theoretically the effect that practical limitations, including damping and limits on the mass and stiffness of the system have on the vibration mitigation performance of the device. We found that, even when physical limitations where in effect, granular chains with local resonances present a significant attenuation of waves propagating at or near the local resonance frequency. We modeled the interaction between the beads using the Hertzian contact law, and the local resonators as mass-spring systems.

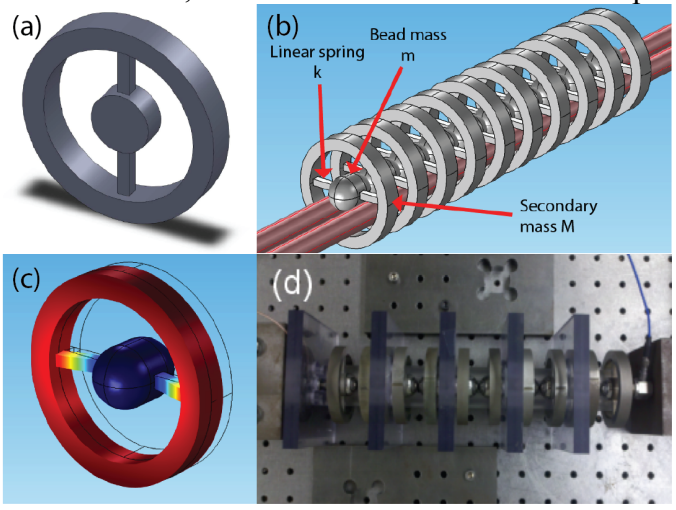

Figure A9.2: (a) 3D model of the local resonator. (b) 3D model of a granular chain where each of the beads contains an embedded local resonator. (c) Vibration profile of the local resonator simulated using a FEM package. (d) Top view of the experimental setup consisting of a chain of ten beads with embedded local resonators.

A10. 1D-elastic: One-dimensional micro-granular lattice

We experimentally studied the wave propagation within ***1D micro-granular chains***. The micro-granular chains were made of two different stainless steel particles (grade 316 and 440c) with diameters of 300 μm. We introduced non-contact excitation and measurement methods to avoid influencing the response of the system with intrusive driving and detection systems. We ensured high-packing repeatability by assembling the micro-particles with a computer-controlled robotic micro-manipulator. To construct one-dimensional chains with micro-particles, we fabricated a one-dimensional supporting micro-structure on silicon wafers to confine the position and motion of the particles. The micro-structures were grooves with a v-shaped cross-section and constrained the particles from moving out of the axis of the groove. We deposited the micro-particles randomly into the v-shaped groove to form a loose chain of particles and then compressed the particles with the computer-controlled micro-manipulator. The position of the micro-particles in the close-packed granular chain was determined using a microscopy imaging system at a 2 μm accuracy.

The mechanical excitation of the micro-particles was achieved by focusing a pulsed laser beam on the surface of selected particles. When we illuminated the particles with laser pulse with sufficient intensity, the induced temperature rise resulted in the vaporization and removal of the particles' surface materials. This phenomenon is known as pulsed laser ablation (PLA) (Fogarassy and Geohegan, 2012) and its efficiency is determined by the material properties as well as the duration and energy of the laser pulses. When ablation was induced on the surface of a micro-particle, the particle obtained momentum through the reaction force from the ablated material. The resulted dynamic response of the micro-particles on the sample stage was measured by two laser vibrometers (Polytec OFV-534).

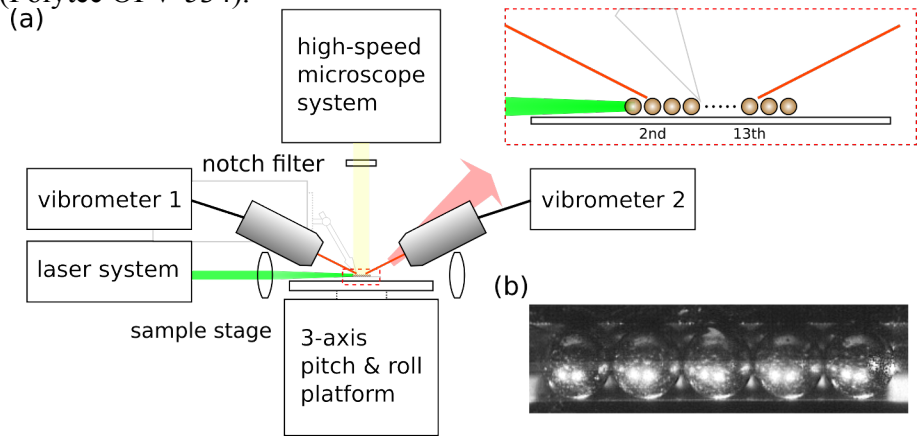

Figure A10.1: Schematic diagram of the experimental setup. (a) Two laser vibrometers were pointed on the assembled micro-granular chain. The granular chain consisted of 15 particles and the vibrometers were pointed at the 2nd and 13th particles. (b) A chain of micro-granular particles was assembled on the sample holder. Particles were placed within a v-shaped micro-structure fabricated on a silicon wafer and compressed with a computer-controlled micro-manipulator.

In experiments, we excited the chain of micro-particles by delivering controlled momentum impulse to its end (the striker). We varied the initial velocity of the striker from 0 to 0.07m/s and measured the responding mechanical motion of the 2nd and the 13th particles in the chain. We also performed numerical study of the system in comparison with the experimental data. The micro-

granular system is modeled with Hertzian interaction between neighboring particles, and the dissipation terms including the Coulomb and air friction which were characterized in our previous work funded by MURI.

A typical measurement obtained by the two vibrometers is shown in Figure A10.2a. The measured vibration is a filtered pulse response function (which is not representative of the real pulse shape because of the bandwidth limits). From the data we extract the maximum amplitudes, $v_{max,1}$ and $v_{max,2}$, of the two velocities output by the 2nd and 13th particles and time delays between the maximum amplitudes Δt. In Figure A10.2b, we plot the measured $v_{max,1}$, $v_{max,2}$ at different striker velocities; the $v_{max,1}$, $v_{max,2}$ shown are normalized to $v_{striker}$. We have averaged the values of $v_{max,1} = (0.57 \pm 0.09)v_{striker}$ and $v_{max,2} = (0.46 \pm 0.07)v_{striker}$. The predicted values obtained in numerical simulations are ${v_{max,1}}^{(simulation)} = 0.89{v_{striker}}^{(simulation)}$ and ${v_{max,2}}^{(simulation)} = 0.64{v_{striker}}^{(simulation)}$. It seems that the measured values are about 40% smaller than the simulation, which might be a result of extra-loss on the striker due to imperfections in the construction of the chain. Finally, we plot the measured group velocity $v_g = (13-2)2R/\Delta t$ at varying striker velocities in Figure A10.2c for both 316 and 440c stainless steel particles. The propagating wave group velocity varies as a function of the striker velocity for both particles tested. This is a clear indication of the nonlinear interaction between the particles. We also plot the simulated results of group velocities in a close packed granular chain with free boundary condition. We note a significant deviation of the group velocities from their predicted values to much lower values. To explain the large deviation of the measured group velocity, we include the presence of gaps between the micro-particles in our simulation. We perform numerical simulations of the wave propagation in a granular chain with randomly distributed gaps between neighboring particles. As seen in Figure A10.2d, when an average gap of 20 nm is included between each contact, the maximum particle velocity along the chain begins to oscillate, and the oscillation amplitude has a variation of about 20%.

We calculate the value of the average group velocity as a function of the striker velocity in the presence of the gaps. The randomly sampled group velocities, at different values of $\bar{\Delta}$ (i.e., mean gaps between particles), are shown as the pink bands in Figure A10.2c. We use a simple equation to estimate the measured group velocity:

$$\frac{2R+\bar{\Delta}}{{v_g}^{(measurement,with\ gaps)}} = \frac{2R}{{v_g}^{(simulation,no\ gaps)}} + \frac{\bar{\Delta}}{v_{striker}}, \qquad \text{(A10.1)}$$

This formula assumes that the total time of flight is equal to the sum of the time required for a wave to travel through the particles and the time required for the free-moving particles to travel the distance of a gap to reach the neighboring particles. The estimated curves obtained from Equation (A10.1) for different gap sizes are plotted by the blue dashed lines in Figure A10.2c and agree well with the corresponding simulation results of the randomly sampled chains.

Our results indicate the very critical role of the inter-particle gaps in the propagation of mechanical wave within a granular chain. As the system size scaling down, construction and assembling of perfect granular system would become increasingly challenging, and our work has demonstrated a functioning non-contact technique to examine and study the mechanical properties in micro-granular system, which can be used for the miniaturization of granular materials.

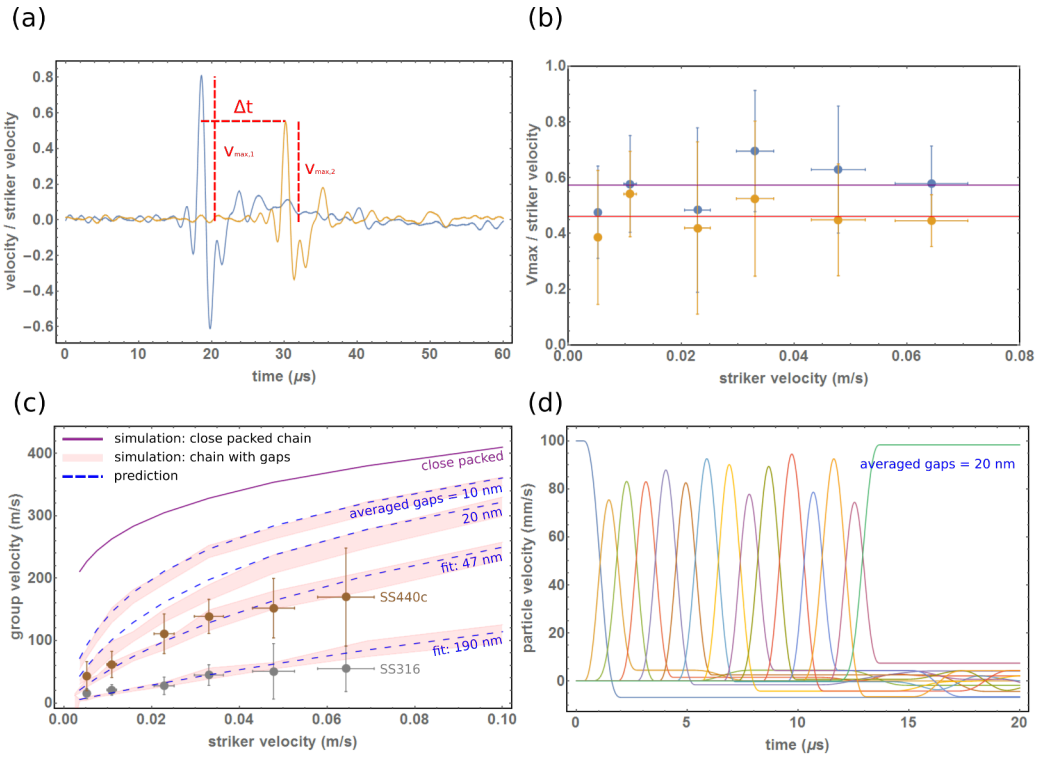

Figure A10.2: Measured particle velocities in a micro-granular chain of 15 stainless steel 440c particles (a) Measured particle velocities for the 2nd and 13th particles in the chain. From these data we obtain the maximum particle velocities, $\boldsymbol{v_{max,1}}$ and $\boldsymbol{v_{max,2}}$, and the time delay $\boldsymbol{\Delta t}$. (b) Measured maximum velocities (normalized to the striker velocity). An averaging gives $\boldsymbol{v_{max,1}/v_{striker} = 0.57 \pm 0.09}$ and $\boldsymbol{v_{max,2}/v_{striker} = 0.46 \pm 0.07}$ (95% confidence interval). (c) Group velocity as a function of the striker velocity, at various gap sizes. Purple line: simulation of an ideal chain (gap=0). Pink bands: simulation results with randomly generated gap distributions, at a fixed average gap size ranging from 10 to 190 nm. Dashed lines: theoretical predictions obtained with Eq. (26), based on the group velocity of a close-packed chain. The measured group velocity is fitted with the simulation results (dashed lines) of systems with averaged gap = 190 and 47 nm for stainless steel 316 and 440c, respectively. The difference in the averaged gap is explained with the different surface roughness of the stainless steel particles we use in experiments. (3 μm for SS316, 0.1 μm for SS440c) (d) Numerical simulations for waves propagating in a granular chain with gaps. The initial velocity is 0.1 m/s and the average gap size is 20 nm

A11. 2D/3D-elastic: Effect of randomness on wave propagation in 1D and 2D granular media

To assess the impact of geometrical and material randomness on the propagation of solitary waves in granular media, the dynamic response of 1D chains of granular media was first investigated. A solitary wave, generated in a semi-infinite perfect granular chain, was propagated through a granular chain with random stiffness and/or mass, and the subsequent evolution and distribution of compressive forces and energy were investigated. Randomness in the granular chain was studied independently by randomizing the distribution in stiffness as $E_i = E_0(1 + r\varepsilon)$ and that in mass as $m_i = m_0(1 + r\varepsilon)$ where E_0 and m_0 respectively correspond to the stiffness and mass of granules in the perfect chain, $-1 \le r \le 1$ is a uniformly distributed random number, and $0 < \varepsilon < 1$ quantifies the degree of randomness. Several idealizations of random chains were averaged to achieve statistical convergence of the numerical results. Figure A11.1 shows typical snapshots of the propagation of the incident solitary wave through the random granular chain with random mass (with $\varepsilon = 0.3$). As apparent there, the solitary wave undergoes a rapid decay due to scattering. Figure (a)-(c) represent the growth of the scattered wave train and progressive decay of the primary wave, which diminishes after forming a silent region.

Analysis of transmitted total compressive force on each bead shows that there are two regimes of wave propagation in the random chain, one characterized by an exponential decay of the primary pulse ($F_m(z)/F_{01} = \exp(-\alpha_F(\varepsilon)z)$) and the other described by a power-law decay driven primarily by the scattered wave train ($F_m(z)/F_{02} = z^{-\beta_F}$). The exponential decay in force (α_F) was found to depend on the degree of randomness ε, but interestingly the power-law decay (β_F) appears to be universal, where the same trend was observed for all degrees of randomness. The two regimes also characterize the transmission of kinetic energy. Utilizing a classical scaling law, the exponential decay coefficient for the kinetic energy is related to its force counterpart through $\alpha_k(\varepsilon) = 5/3\alpha_F(\varepsilon)$. This expression was found to be in very good agreement with the numerical results. This work was summarized in (Manjunath *et al.*, 2012).

This 1D work was then extended to 2D dimer crystals made of a square lattice of larger spheres with smaller interstitial masses. In that study, the source of randomness associated with the mass of the components. As observed in the 1D case, two randomness-induced regimes of decay are observed, in addition to the decay associated with the multi-dimensional nature of the wave propagation (Figure A11.2).

A detailed study of the directional nature of the spatial decay of the waves showed a marked transition between the anisotropic decay observed for the non-random system and the increasingly isotropic decay obtained for higher level of randomness. The 2D work on the effect of randomness was summarized in (Manjunath *et al.*, 2014a) and (Leonard *et al.*, 2012).

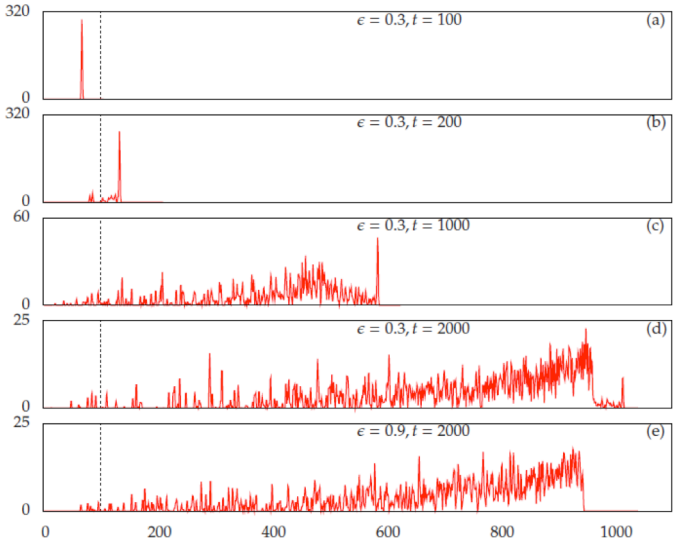

Figure A11.1: Evolution of an incident solitary wave through a random granular chain. The primary pulse progressively decays due to the scattering associated with the property mismatch between adjacent spheres. For a while, a silent region is generated behind the primary pulse, which is eventually overtaken by the scattered wave train.

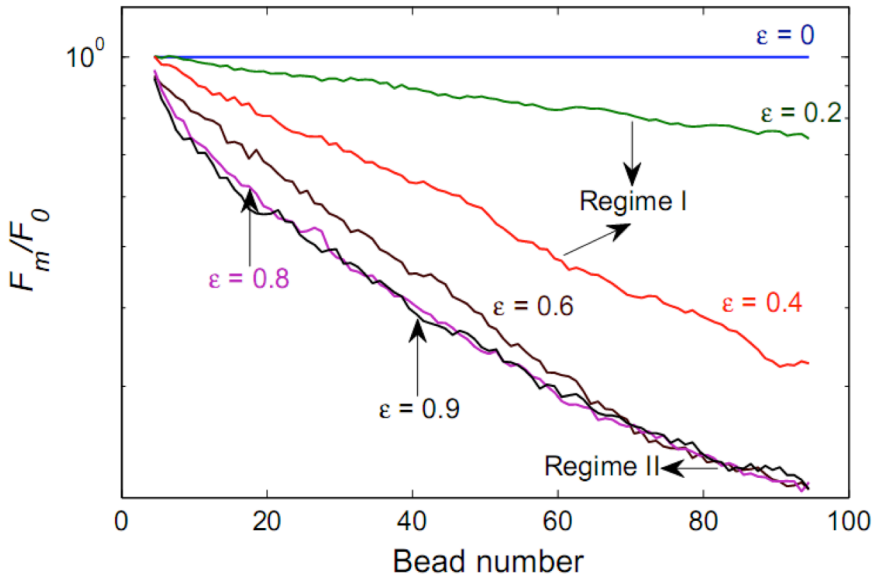

Figure A11.2: Effect of randomness on the propagation of a impact-induced wave in a 2D granular medium: spatial evolution of the maximum amplitude of the wave (after extraction of the effect associated with the dimensionality) for various values of the random parameter ε. ε=0 denotes the non-random solution.

A12. 2D/3D-elastic: Plane wave propagation in ordered granular media

This aspect of the research project has shed important light on a wide variety of fundamental wave propagation phenomena in 2D granular crystals, with emphasis on plane wave problems. In the first set of studies presented in (Manjunath *et al.*, 2014b), we derived a universal law for the relation between the velocity of a planar solitary wave and the amplitude of the maximum force amplitude of the wave. As shown in Figure A12.1, this relation is valid for 1D, 2D and 3D ordered granular systems made of spherical particles interacting elastically. This relation is an explicit function of the material properties (Young's modulus and Poisson's ratio) and geometry (radius) of the beads, and the packing geometry (distance between adjacent layers and number of contacting beads).

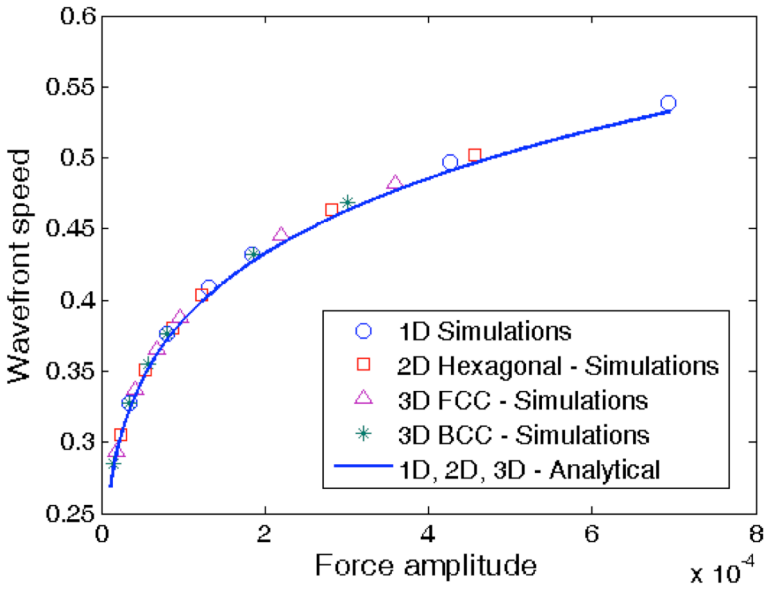

Figure A12.1: Universal relation between wave speed and force amplitude for a solitary plane wave propagating through 1D, 2D or 3D granular media. The symbols correspond to numerical results, while the solid curve corresponds to the analytical expression.

A second set of studies then focused on the incline plane loading of mono-disperse granular crystals (Figure A12.2). This work showed for the first time how the shear component of the plane wave rapidly decays as the wave penetrates into the granular medium, while the normal component of the wave propagates as a solitary wave, i.e., without decay over long distances. This behavior, which is reminiscent of the exponentially decaying Rayleigh surface waves in linearly elastic solids, was investigated numerically and analytically. Some of the results are illustrated in

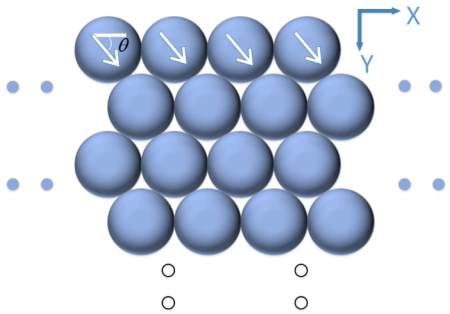

Figure A12.2: Inclined plane loading of a hexagonal close pack of spheres.

Figure A12.3: the left figure presents the evolution of the contact force between two adjacent beads located in various layers (with Layer 1 representing the surface layer), showing how the forces even out after about 10 layers. The right figure presents the rapid decay of the horizontal velocity component for an inclined loading (with angle = 60°), showing the existence of different regimes of decay, starting from purely exponential (R1) to an inverse decay (R2 to R4).

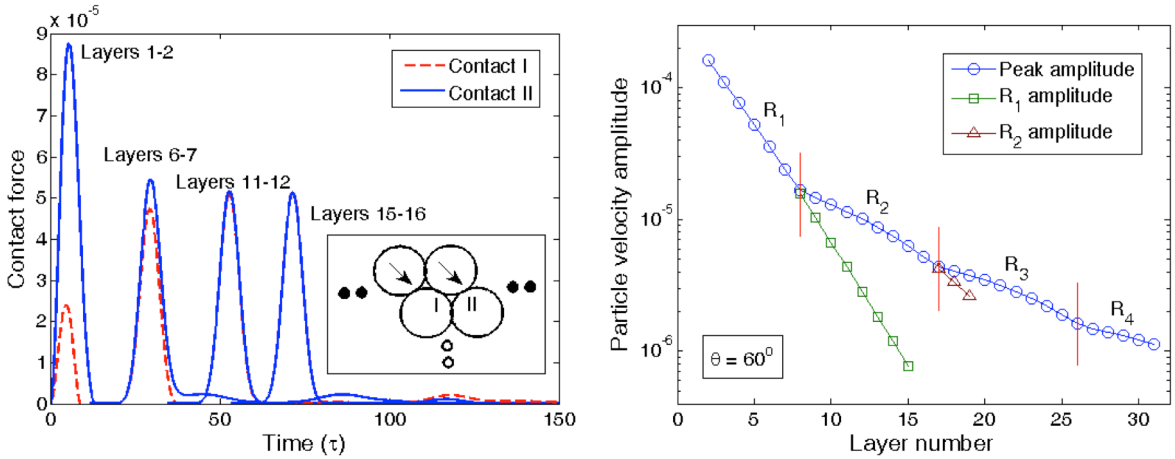

Figure A12.3: Inclined planar impact of hexagonal granular crystal, showing how the peak contact forces acting on adjacent spheres even out after about ten layers (left) and the decay regimes of the horizontal component of the velocity.

An analytical expression of the force-velocity relation for the solitary wave component of the inclined planar loading was also derived and compared with numerical simulations, showing excellent agreement (Figure A12.4) for all impact angles considered.

This work on the inclined plane loading of mono-disperse granular media is also summarized in (Manjaunath *et al.*, 2014b).

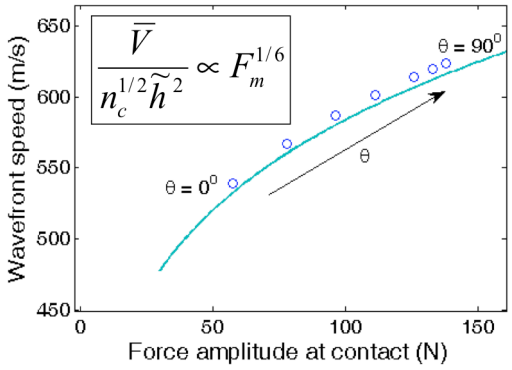

Figure A12.4: Force vs. velocity relation for solitary waves generated through a planar impact on a granular crystal, with the impact direction inclined by an angle θ. Symbols: numerical, Curve: analytical.

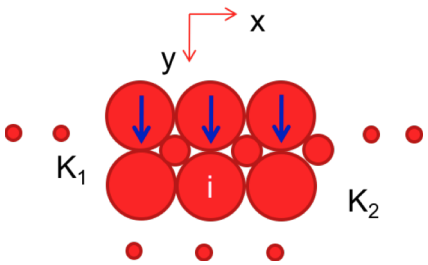

Figure A12.5: Planar impact of dimer granular crystal made of elastic spheres.

In the last study related to plane wave propagation in ordered granular media, we tackled the problem of normal impact loading of dimer square-packed systems (Figure A12.5), characterized by two contact stiffness values (denotes by K_1 and K_2 in the figure). We first demonstrated the existence of a non-local 1D model with the same wave propagation characteristics as the 2D granular crystal, but with a scaled value of the contact stiffness K_2 characterizing the contact between larger and smaller spheres. Using this simplified nonlocal model, we showed the existence of a new family of solitary waves expressed in terms of the two non-dimensional parameters that define the mass ratio (ε) and stiffness ratio (α) present in the problem.

The existence of this new family of solitary waves was first demonstrated numerically by simulating wave propagation in a non-local 1D granular chain. The outcome of this study is shown in Figure A12.6, which presents the set of dimer systems that sustain solitary waves (solid curves) together with a set of material combinations (symbols).

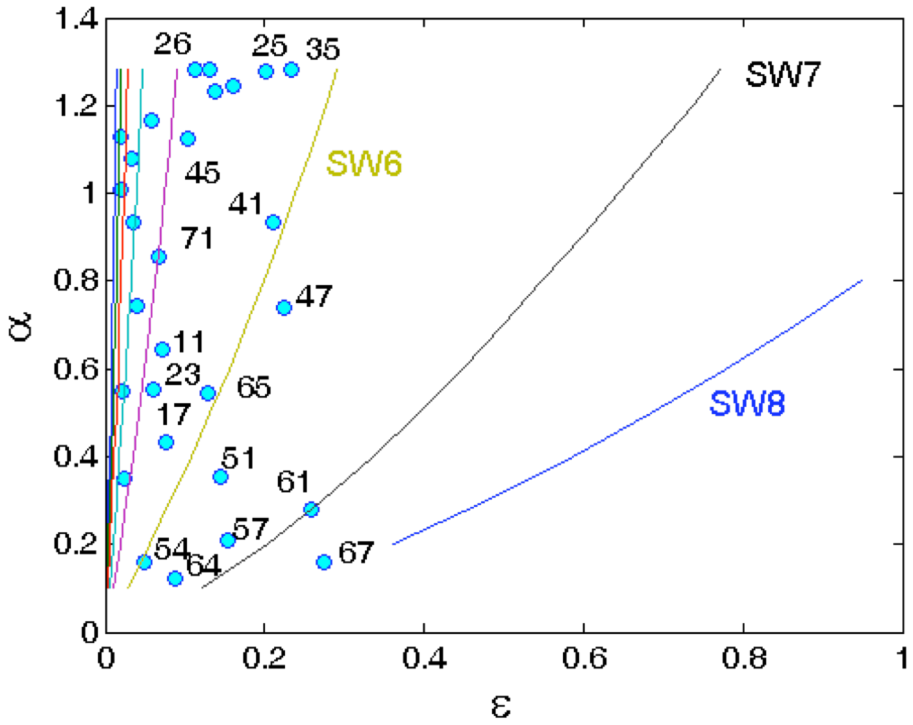

Figure A12.6: Solitary waves in a granular dimer crystal defined by the mass ratio ε and the stiffness ratio α. The solid curves denote the (α,ε) values giving rise to solitary waves. The symbols correspond to actual material pairs, with the first digit denoting the larger particles and the second the smaller ones. 1=stainless steel, 2=delrin, 3=polycarbonate, 4=aluminum, 5=alumina, 6=PTFE, and 7=brass.

This new family of solitary waves was then studied with the aid of an asymptotic analysis valid for small values of the mass ratio ε. Typical results from this analysis are presented in Figure A12.7. The left figure shows a comparison of the velocity profile of the solitary wave

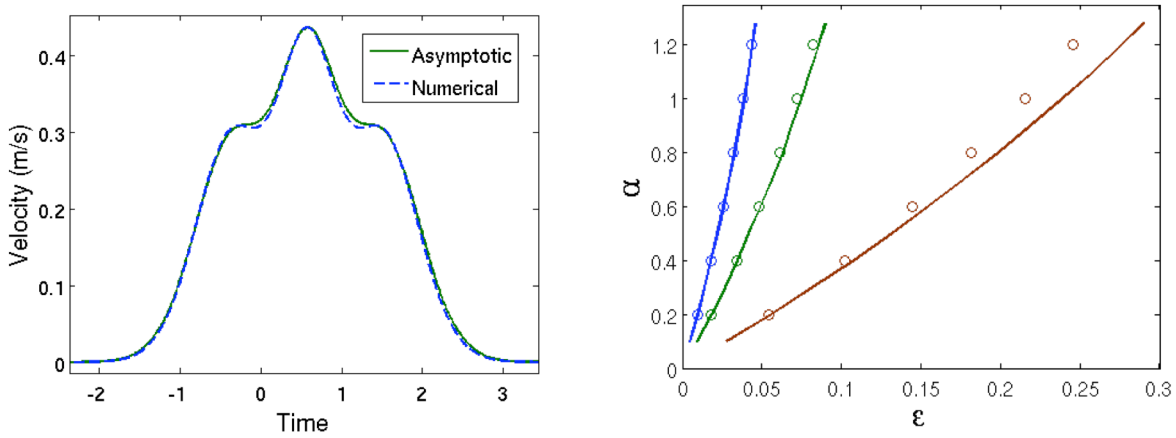

Figure A12.7: Left: Asymptotic and numerical estimates of the evolution of the small particle velocity associated with the passage of a solitary wave for ε=0.0274 and α=0.644. Right: Comparison between numerical (circles) and asymptotic (solid curves) estimates of the locus of three groups of solitary waves, showing excellent agreement especially for small values of the mass ratio ε on which the asymptotic analysis is based.

obtained numerically (dashed curve) and analytically (solid curve) for the case ε=0.0274 and α=0.644. The right figure compares numerical (circles) and asymptotic (solid curves) estimates of the locus of three families of solitary waves in the (α,ε) plane. This work is summarized in (Manjunath *et al.*, 2014c).

A13. 1D-plastic: "Solitary-like" plastic waves in 1D granular chain

Experiments were conducted to investigate the propagation of disturbances in 1D granular media when the applied force was increased to such levels that material nonlinearity, in the form of plasticity, would become important. These granular media were loaded by a modified split Hopkinson pressure bar (SHPB) with a momentum trap. The trap ensures the granular chain is *loaded only once*, allowing more accurate post-mortem measurements to be made. Chains of brass beads of increasing length were studied, and their transmitted force for similar input loading is compared in Figure A13.1a. As the number of beads in the chain increases, the duration of the transmitted pulse increases. Even though the input load has the same 80 ms duration in all cases, although not necessarily exactly the same amplitude, the resulting transmitted pulse duration is variable. Note that the transmitted pulse duration for chains with two or three beads, is shorter than that of a single bead, and of the loading pulse duration. This result was seen consistently for repeated tests of two and three beads, and the reason for it is not clear. However, this "transition" occurs at the same time as the amplitude of the first and second peaks reverses in magnitude. As chain length increases, the two peaks, which correspond to the yielding of individual contact points, also begin to converge into a single peak. This becomes apparent in the four, and especially the five, bead case. As the number of beads increases, the transmitted pulse also begins to attain a trailing pulse of lower amplitude.

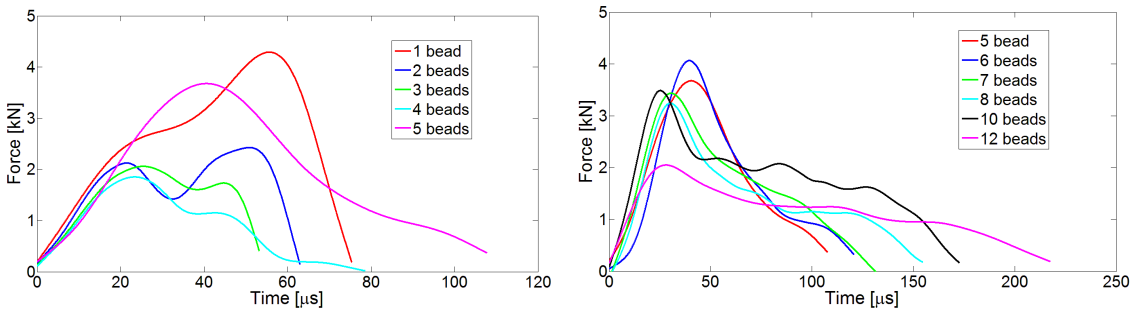

(a) (b)

Figure A13.1: Transmitted signals for brass bead chains of length (a) 1-5, (b) 5-12.

This trailing wave is more apparent in Figure A131.b, which shows the transmitted pulse for longer chain of beads, from 5 to 12 brass beads in length. The duration of the transmitted stress wave increases as the granular chain length increases. The increasing duration of the transmitted signal in the granular case is produced by a combination of the nonlinear contact between beads and the effect of plasticity, and may be useful in stress wave management and mitigation applications. It can be seen that the magnitude of the transmitted force decays with chain length. This can be attributed to the additional plasticity involved with the additional beads, which will lower the final force that reaches the transmitted bar. *Based on the results of Figure A13.1, it can be concluded that* ***the number of particles necessary to set up a plastic solitary-like wave is about 5, as is also the case for the elastic granular chain***.

Nesterenko (1984) described solitary waves forming under a chain of identical elastic beads with the velocity also scaling with $F_{max}^{1/6}$ when no initial pre-compression exists. This relation is compared to the experimental results of brass chains loaded dynamically. The measured wave speeds for chains of more than 5 beads are plotted against the maximum transmitted force in Figure A13.2. Power laws fitted to the experimental data are compared. The experimental velocity does not appear to scale with $F_{max}^{1/6}$, but rather approaches $F_{max}^{1/9}$ instead.

This is an effect of plasticity which can have additional damping effects on the solitary wave generation. However, it is clear that the speed does depend on the output force, denoting that a nonlinear wave is propagating after chain lengths of 5 beads.

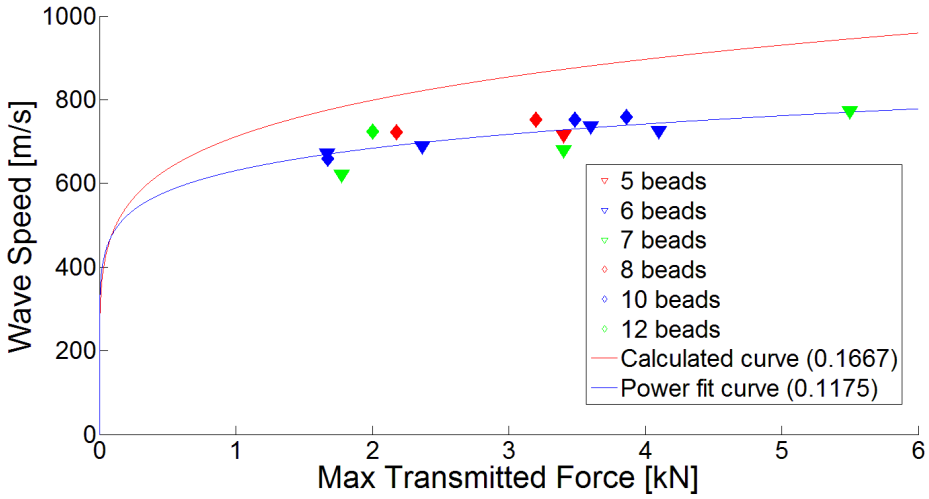

Figure A13.2: Wave speed vs. maximum transmitted force for various brass bead chains.

By analyzing the propagated wave for different chain lengths, and comparing these signals as the chain length increases, a transition in wave behavior was identified. Similar to the elastic case, the critical length for this transition resides between four and five beads. After this critical length, for similar input amplitude and duration, the transmitted wave decayed in amplitude as the chain length increased. Also, the duration of the transmitted wave increased with chain length.

PART B – DEMONSTRATION: MATERIAL DESIGN

B1. 2D/3D-elastic: Wave tailoring in 2D dimer crystals

In this study summarized in (Awasthi *et al.*, 2012), we investigated how to tailor wave propagation in a dimer granular crystal by modifying the mass and stiffness ratios between the larger and smaller spheres. The analysis was performed numerically using the molecular dynamics solver LAMMPS specially adapted for the simulation of granular media, with the inter-particle interactions described by the nonlinear Hertzian contact relation. The analysis characterized the propagation behavior of point-impact-induced waves in a granular material as illustrated in Figure B1.1. The left figures illustrate four wave propagation profiles ranging from a clearly defined solitary wave propagating quasi-isotropically (top left) to a very directional wave propagation regime (bottom right). The right figure shows a summary of the propagation regimes on the mass ratio vs. stiffness ratio space. The symbols correspond to the cases investigated numerically, and the dashed curve denotes the analytical prediction of the limits of the solitary wave regime.

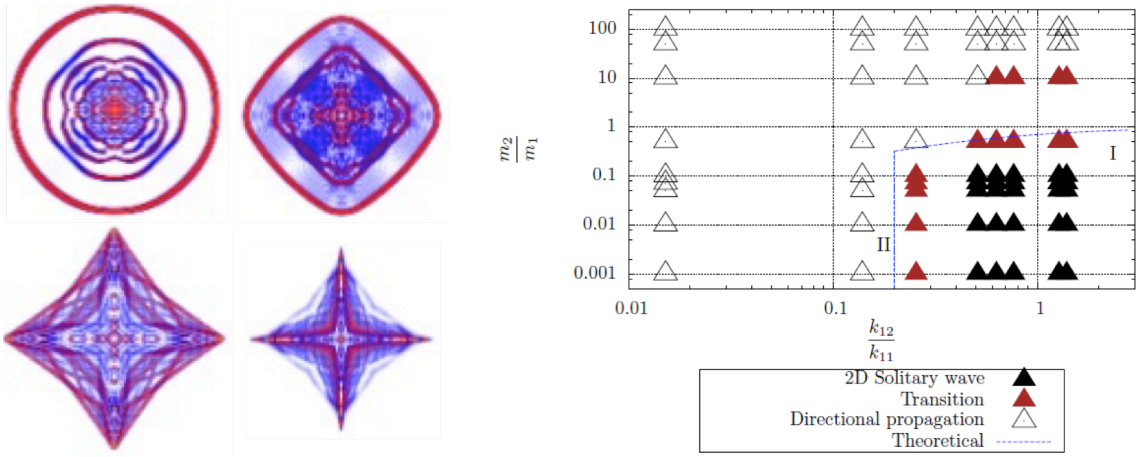

Figure B1.1: Left: Modes of wave propagation observed for different combinations of mass and stiffness ratios. Right: Modes of wave propagation mapped over the mass/spring constant ratio space. The blue contour shows the theoretical prediction of the bounds of the solitary wave regime, denoted by dark triangles in the numerically extracted map.

The impact of the directionality of the wave propagation in granular media was also investigated in the case of force transmission across a granular layer in (Awasthi *et al.*, 2015).

B2. 1D-plastic: Characterization and mitigation of plasticity at inter-particle contacts

Due to the presence of stress concentration at the contact between spherical particles, inelastic effects are often unavoidable for impact load exceeding a few hundred Newtons. In this part of the project, we performed a detailed investigation of the impact of plasticity in the propagation of waves in granular chains and crystals made of elastic-perfectly-plastic spheres.

The first part of this work was the derivation of an accurate contact model that included plastic dissipation. This derivation was performed using a detailed finite element analysis with Abaqus (Figure B2.1) for a range of material properties (e.g., yield stress) and particle size ratios.

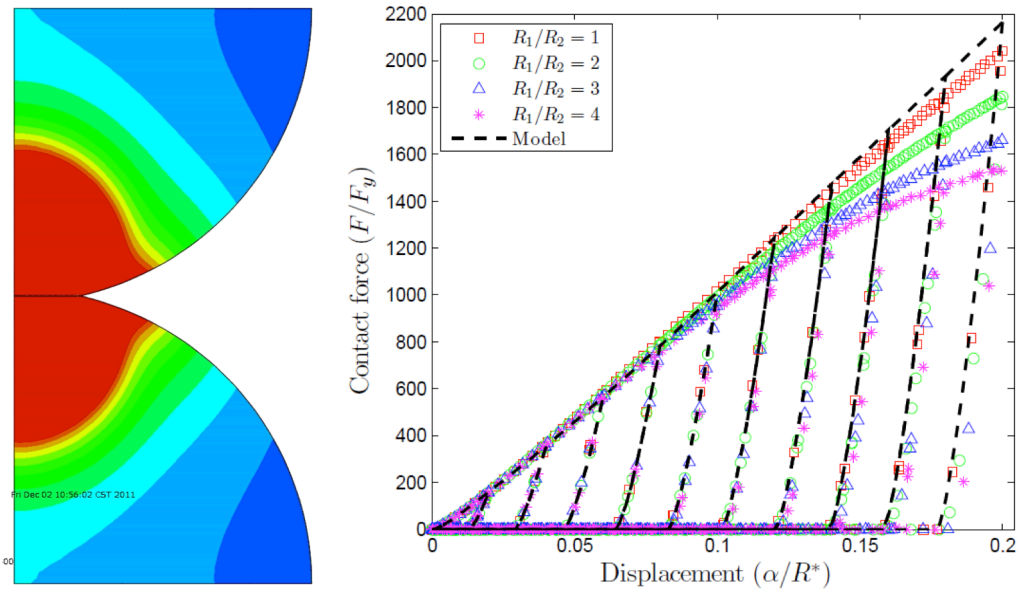

Figure B2.1: Extraction of an elasto-plastic contact law for spherical particles. Left: Finite element analysis performed with Abaqus, with the red contour denoting . Right: Comparison between numerical and analytical force-displacement curves obtained for four values of the particle radius ratio, showing good agreement up to relatively large values of the relative displacement α between the particles. F_y denotes the critical force value associated with the onset of plasticity.

The numerical studies involved a set of loading and unloading steps of increasing amplitudes to capture the complete history of contact during the passage of an impact wave.

The resulting elasto-plastic contact law was then implemented into LAMMPS, thereby allowing for the simulation of larger granular systems. In particular, it allowed for a comparative study of the energy dissipation associated with an impact event in a granular medium and in a continuum medium made of the same elasto-plastic material. As part of that study, scaling laws were

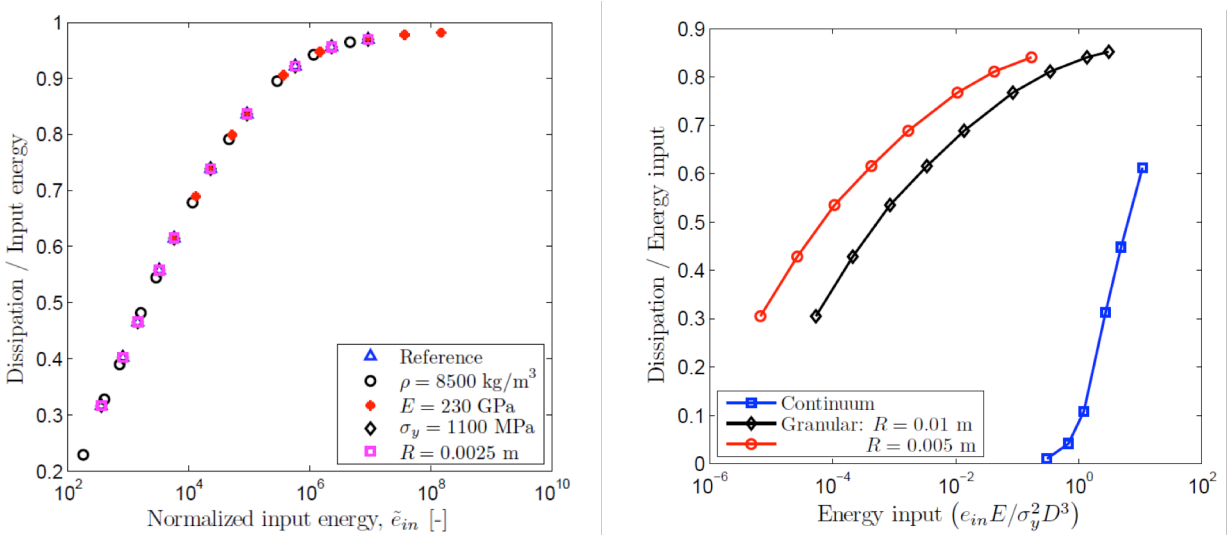

Figure B2.2: Left: Energy dissipation ratio vs. normalized input energy for a point impact on an elasto-plastic granular medium. The scaling law derived for the input energy ($\tilde{e}_{in} \sim \left(\frac{E^4}{R^3\sigma_y^5}\right) e_{in}$) allows for all the curves to collapse on a single master curve. Right: Energy dissipation vs. energy input: comparison between continuum and granular systems, showing the ability of the elasto-plastic granular media to dissipate impact energy at load levels substantially lower than those for a continuum medium.

derived from first principles to capture the effects of key quantities such as Young's modulus, yield stress, and particle/impactor diameter. An example of scaling law is shown in Figure B2.2, which presents the master curve of relative energy dissipation vs. the input energy for granular elasto-plastic media corresponding to various values of the density, Young's modulus, yield stress and particle diameter. The right figure provides a direct comparison between the ability of elasto-plastic continuum and granular media to dissipate energy. As indicated there, the granular medium dissipates the impact energy at energy input levels that are substantially less than those associated with a continuum medium made of the same material. This difference is associated with the presence of stress concentrations at the particle-to-particle contacts.

This line of work on the effect of plasticity on wave propagation in granular media, including the effect of introducing an elasto-plastic intruder in an otherwise linearly elastic granular chain, has been summarized in (Pal *et al.*, 2014a), (Pal and Geubelle, 2014a), (Pal *et al.*, 2014b).

To experimentally validate the elasto-plastic contact law we performed a series of specially designed experiments to investigate the dependence of plastic contact law on bead material, size, and combination, and to establish the importance of material rate sensitivity in the dynamic contact law. The SHPB apparatus was used to generate a dynamic loading at different levels. A lead pulse shaper was used to smooth the incident pulse and the momentum trap technique was again applied to prevent multiple loadings on the specimen. In order to obtain the dynamic elasto-plastic contact law between spherical particles, a two-hemispherical-bead

specimen setup is proposed, as shown in Figure B2.3, which allows loading a *single* point contact. From the SHPB data, the dynamic force and the displacement between the two centers of the hemispherical beads can be measured.

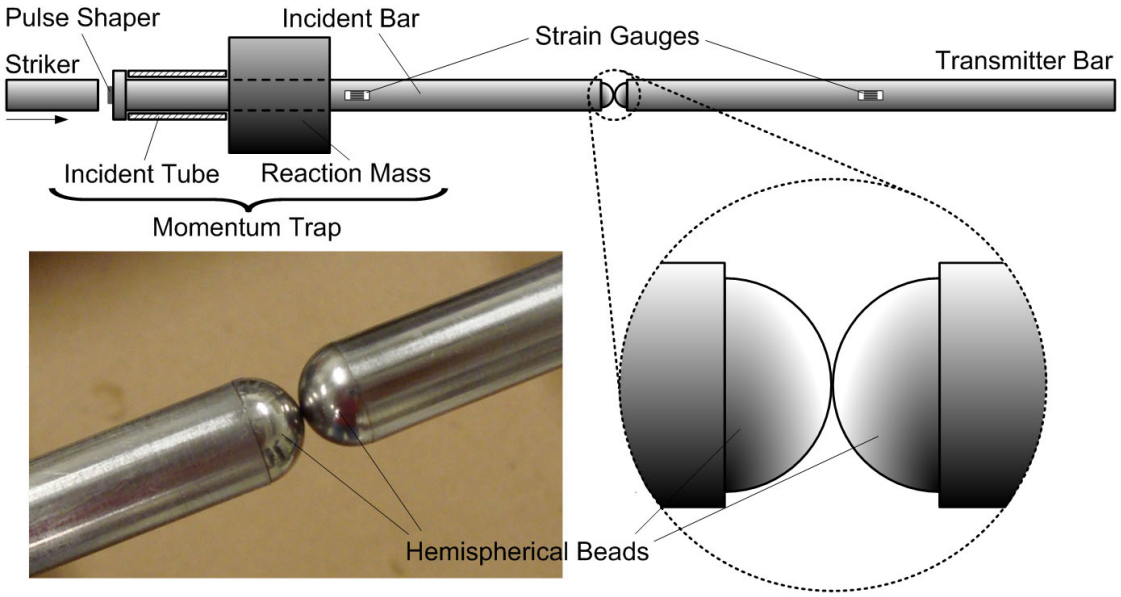

Figure B2.3: The SHPB apparatus modified for studying the dynamic load-displacement contact law of a single contact.

The experimental quasi-static and dynamic contact load-displacement curves for a point contact between identical beads with a diameter 9.525 mm are shown in Figures B2.4 and B2.5. For strain rate insensitive materials such as aluminum or brass (Figure B2.4), the quasi-static and dynamic contact load-displacement curves are also rate insensitive. This indicates that the point contact behavior of the beads is not affected by loading rate.

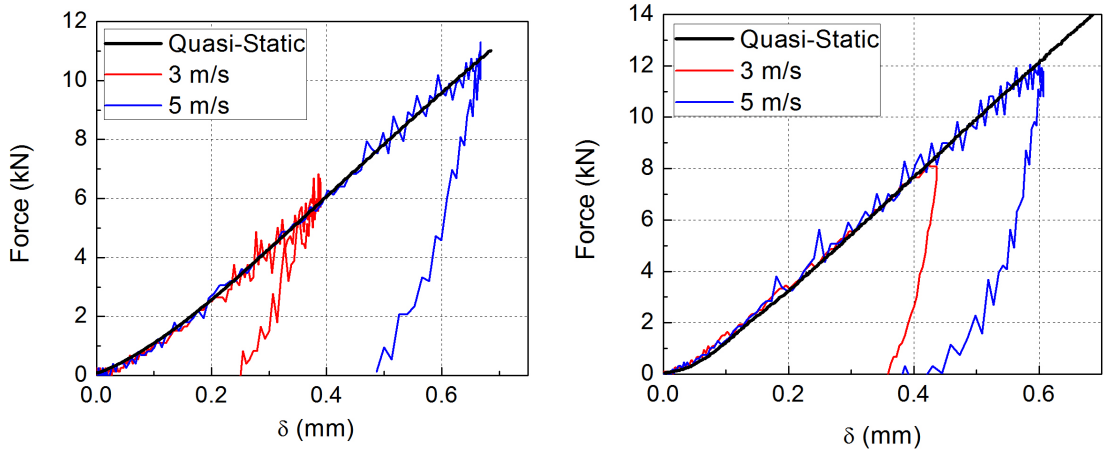

(a) Aluminum alloy 2017 (b) Brass alloy 260

Figure B2.4: Contact load-displacement curves for strain rate insensitive materials

For strain rate sensitive materials (Figures B2.5), the slope of the plastic part has an obvious increase as the loading rate increases. It shows clearly that the loading rate does affect the

dynamic single-point contact behavior. Another parameter that affects the contact law is the sphere size.

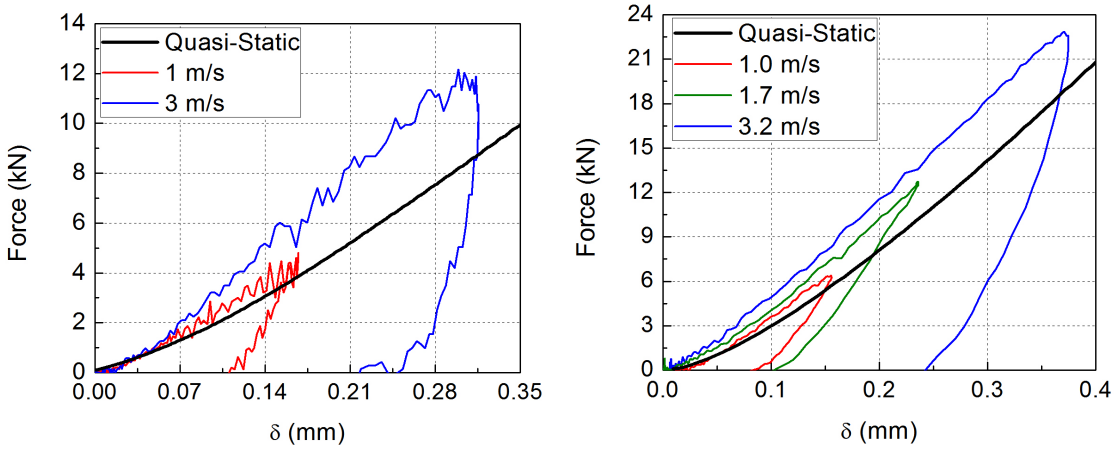

(a) Stainless steel 302 (b) Stainless steel 440c

Figure B2.5: Contact load-displacement curves for strain rate sensitive materials

B3. 1.5D-elastic: Design of confined granular systems for wave tailoring (Acoustic Switch)

A variety of confined granular systems have been investigated as practical implementations of wave tailoring systems. An example of such system investigated in (Pal and Geubelle, 2014b), shown in Figure B3.1, consists of a chain of larger spheres in contact surrounded by 6 to 9 'circumferential spheres' also in contact and confined by a rigid cylinder. By controlling the confinement level (defined by the relative radial displacement $a=\delta_0/D$), an impact-induced wave traveling down the primary chain of larger beads can be tailored from quasi-solitary wave (i.e., without dissipation) to rapidly decaying. This result is illustrated in Figure B3.2,

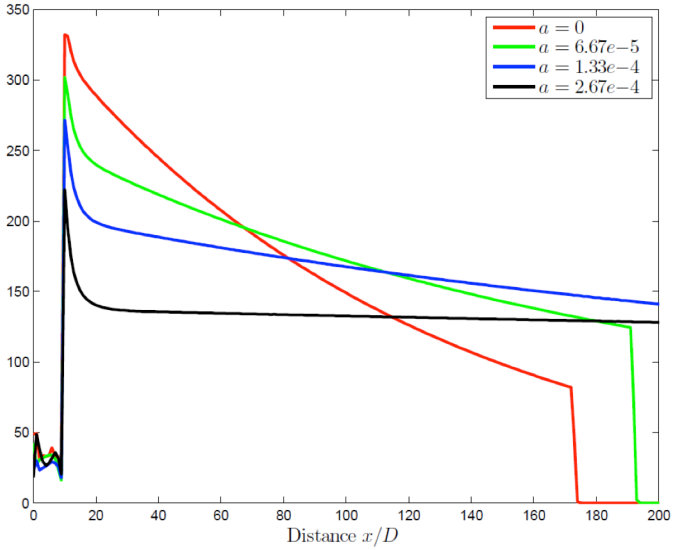

Figure B3.2: Wave tailoring achieved with the confined granular system shown in Figure B3.1 with eight circumferential spheres. As the level of confinement (defined by the non-dimensional parameter $a=\delta_0/D$) is increased, the contact force goes from rapidly decaying (red curve) to quasi-solitary (black curve).

which shows the spatial evolution of the maximum amplitude of the wave as it travels down the granular chain.

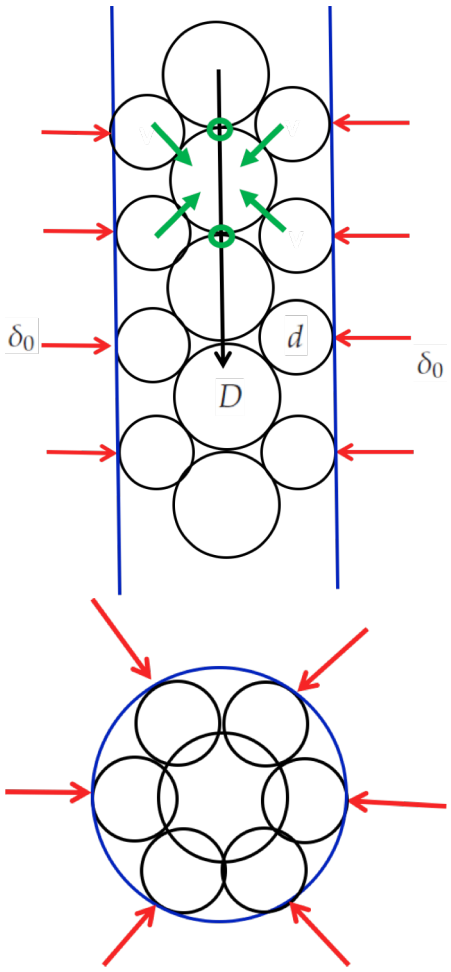

Figure B3.1: Wave tailoring medium composed of a chain of larger spheres confined by sets of six smaller spheres and a rigid cylinder. By adjusting the confinement δ_0, a wave traveling down the center chain can be maintained or attenuated.

A practical implementation of these phenomena was done in what we term a *gravity assisted acoustic switch* which introduces a framework for wave tailoring based on changing the relative positions of granules, i.e., the lattice network, between two configurations. Here the lattice is arranged in a plane and wave propagation is considered in the axial direction only, i.e., what we call quasi-1D or 1.5D. Schematics of the two configurations are illustrated in Figure B3.3 for both side and top views. The lattice consists of both a 1D primary chain of spheres –

"axial spheres" that are aligned with the impact source (red in the figure), and "side spheres" which are symmetrically placed on opposite sides of select axial spheres (blue in the figure). The side spheres are confined between two rigid parallel plates. The lattice attains two states based on its inclination relative to the impact direction. In the downstream configuration shown in Figure B3.3a, the lattice is inclined such that a pair of side spheres are in contact with the adjacent axial sphere downstream (defined as the direction of primary pulse propagation) and a gap exists between the pair of side spheres and the axial sphere upstream. In the upstream configuration shown in Figure B3.3b, the lattice is inclined such that a gap exists between a pair of side spheres and its adjacent axial sphere in the downstream direction. Switching between the two configurations can easily be achieved by slightly tilting the lattice in one of two way in a gravitational field, as illustrated in the lower part of Figure B3.3.

When the downstream configuration (Figure B3.3a) is impacted along the axial direction, there is a solitary wave propagating through the chain. The axial spheres moving forward do not contact the side spheres ahead as the wave propagates and the side spheres play no role in the dynamics of the lattice. In contrast, when the upstream configuration (Figure B3.3b) is subjected to an impact, a wave with progressively decaying amplitude traverses through the lattice as the wave interacts both with the spheres along the axis and the side spheres. After impact, the side spheres are in free flight and they eventually collide with the spheres and there are local oscillations. The energy lost due to these local oscillations is similar to the oscillations observed in wave propagation through dimer lattices (studied elsewhere in this project) at the tail of the propagating wave where the smaller mass of a dimer unit cell may oscillate between two larger masses.

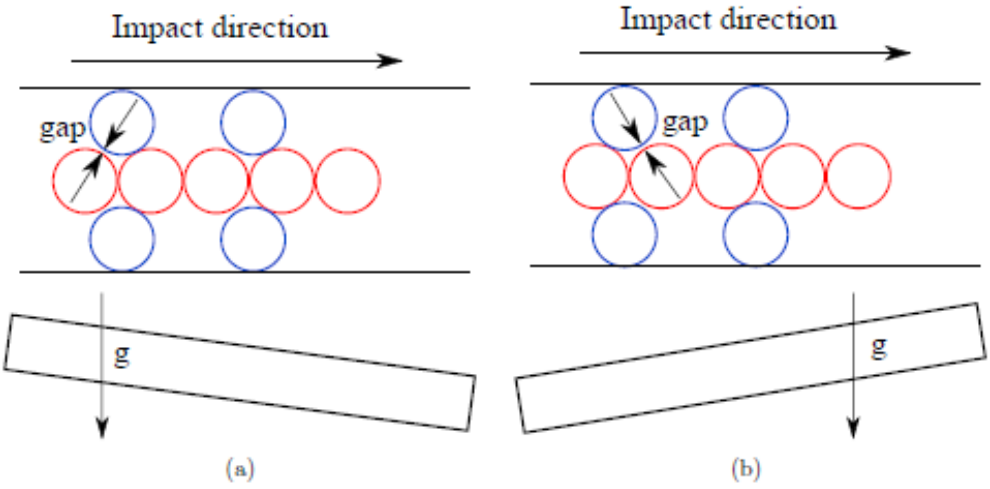

Figure B3.3: Schematic with top and front views illustrating the concept of altering the lattice network topology by gravity. (a) Side spheres (red) contact axial spheres (red) in the axis in impact direction, and (b) side sheres contact the spheres in the axis downstream, resulting in distinct axial wave propagation

Note that the difference between the two configurations is in the location of the side spheres along the chain. The key aspect in our design is a change in lattice network topology, causing a change in the wave propagation behavior from a solitary wave to a rapidly decaying wave down the primary chain. Thus, our configuration is analogous to atoms shifting positions, for instance a phase transformation in a shape memory alloy, resulting in a change in effective material properties. We further remark here on the generality of our proposed framework. Indeed,

other configurations may also be designed to change the lattice network and have the desired effect. For instance, moving the walls inward to achieve a gap between the central spheres so that there is a rapidly decaying wave along the chain. On the other hand, moving the plates outward, so that the side spheres are no longer in contact with the axial spheres would allow a solitary wave to propagate through the chain.

Figure B3.4a illustrates both the numerical and experimental results for the velocity of the final sphere in an impacted chain, normalized with the velocity of the impacting sphere, for the *upstream* configuration. The experimental data for each set of pairs of side spheres are in good agreement, demonstrating the repeatability of our experiment. The leading wave loses energy at each side sphere contact, resulting in progressive decay of the wave amplitude with number of pairs of side spheres. The energy loss is due to the transfer of energy from the axial to the side spheres at each contact location. The velocities obtained from the corresponding numerical simulations are a bit higher than the experimental measurements, but the trends are very similar. We note there assumptions in our model here which may lead to higher velocities: The contacts are assumed to be frictionless and the walls are assumed to be perfectly rigid, i.e., no energy is radiated outward to the walls. Also friction between the side spheres and the wall can reduce the output velocity by a small amount, however, the trends are qualitatively similar.

Figure B3.4b illustrates the peak forces at the same sphere for different numbers of side sphere pairs when the chain is in the *downstream* configuration. The forces are normalized by the force acting on the first sphere, which is calculated based on the impact velocity. A solitary wave propagates down the chain independent of the number of pairs of side spheres. The axial spheres do not interact with the side spheres as their displacement toward the impact direction is about 13 μm, which is much less than the gap between them and the side spheres. Again, the forces due to numerical simulations are observed to be higher than that observed experimentally, due to the aforementioned reasons. Figures B3.4a,b demonstrate that the behavior is significantly different between the upstream and downstream configurations, thus validating our proposed design for an acoustic switch that can go between passing acoustic waves and attenuating them simply by a small change of its tilt in a gravitational field.

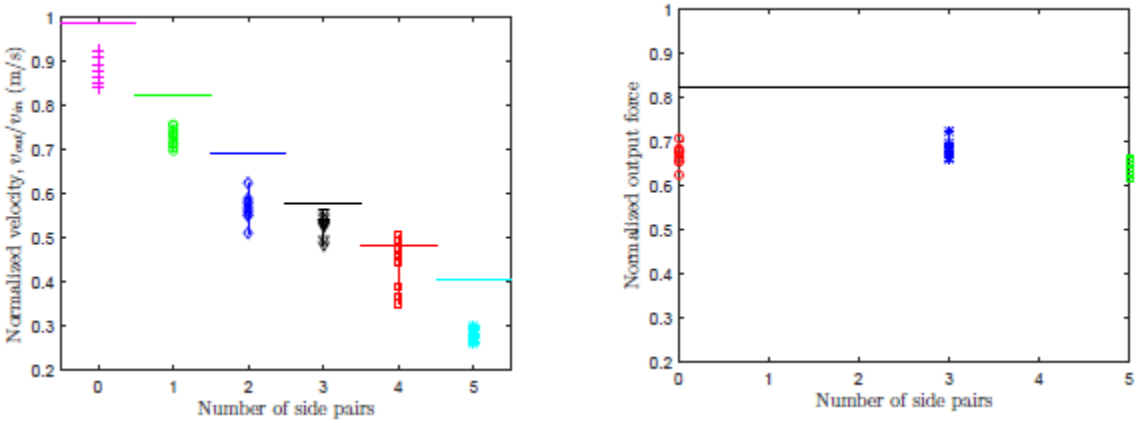

Figure B3.4: (a) Upstream configuration – experimental (points) and numerical (solid lines) values show that the output velocity decreases rapidly with increasing side pairs. (b) Downstream configuration – experimental (points) and numerical (solid line) values of peak forces show that the force experienced at the 18th bead is constant regardless of the number of side pairs.

B4. 2D-plastic: Elasto-plastic wave propagation in 2D granular packing with preconditioned beads

Another important contribution to this work has been the introduction of the concept of ***preconditioning***, which has been proposed to alleviate the effect of plastic dissipation by pre-conditioning pairs of particles to a pre-defined level of static loading. The concept, which is illustrated in Figure B4.1, allows for elastic contact at much higher load levels, at least two orders of magnitude higher than those attainable by non-preconditioned beads. This concept, which has been presented both analytically and experimentally in (Wang *et al*., 2014), also offers the potential for force filters, as loads exceeding the pre-conditioning force (denoted by point B in Figure B4.1) will be damped out, while those lower than this can propagate through the granular chain. In addition to demonstrating the concept of preconditioning in Wang *et al*., (2014) a further objectives of this part of the effort was to **s**tudy the propagation of elasto-plastic wave in 2D granular packing with preconditioned beads, and compare the results to that in non-preconditioned bead packings. All preconditioned beads were generated manually – a time intensive process that would have to be improved in any future applications. The bead to be preconditioned, made of brass alloy 260, was first sandwiched between two parallel flat loading heads as shown in Figure B4.1 and then quasi-statically loaded beyond yield to given preconditioned load levels. In the current study, the preconditioning level was set at 9 kN. The bead was subsequently unloaded, producing two preconditioned areas at opposite sides of the bead.

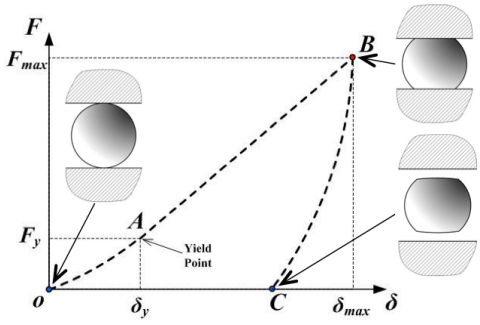

Figure B4.1: Preconditioning process

After preconditioning, the beads were assembled with the preconditioning direction parallel to the horizontal in a 2D hexagonal packing consisting of 11 layers alternating between rows of 9 and 10 beads (the first and last rows all contain 10 beads) as shown in Figure B4.2. Note that in this configuration the contacts along the 60 degree direction are still with original, i.e., non-preconditioned, contact radius. Therefore, the horizontal direction of this 2D packing can elastically sustain any load less than 9 kN, while all of the 60 degree angle contacts would yield at a very low force level (around 125 N based on the modified Thornton model for this material). A split Hopkinson pressure bar apparatus was then used to impact the specimen to generate an elasto-plastic wave. A in-house designed 1018 low carbon steel frame was built to hold the 2D granular packing and enable fixed boundary conditions all around. Several piezoelectric sensors were embedded in specific beads to obtain the force profiles of waves travelling through the array. The beads were carefully inspected for the yield locations after each experiment.

The force profiles were measured from a total of six different locations in the 2D preconditioned bead packing. Typical force profiles from three locations are shown in Figure B4.3. For comparison, the force profiles measured at the same locations in a non-preconditioned bead packing are also shown in Figure B4.3. The signals have been aligned based on the impact time at the impact location. It can be seen that the sensor 1 signal, which is the signal at the horizontal direction, in the preconditioned bead packing has a much higher primary peak than that in the non-preconditioned case. The arrival time in the preconditioned bead packing is also earlier than in the non-preconditioned one. This indicates that the preconditioning treatment in

the horizontal direction increases the load carrying ability of the contact point and consequently transfers higher amplitude and higher speed solitary waves in this direction. In contrast, the sensor 3 signal, which is the signal in the vertical direction opposite impact, is comparable or even lower in the preconditioned case than that in the non-preconditioned packing. This indicates that the preconditioning treatment in the horizontal direction does not help to transfer less energy in vertical direction although it does transfer higher forces in the horizontal. The primary peak force and the arrival time of the force profiles from all six sensors used are summarized in Figure B4.4. Though the data show significant scatter due to the randomness inherent in these 2D experiments, the signals at sensor 1 location still clearly show higher primary peak and earlier arrival times.

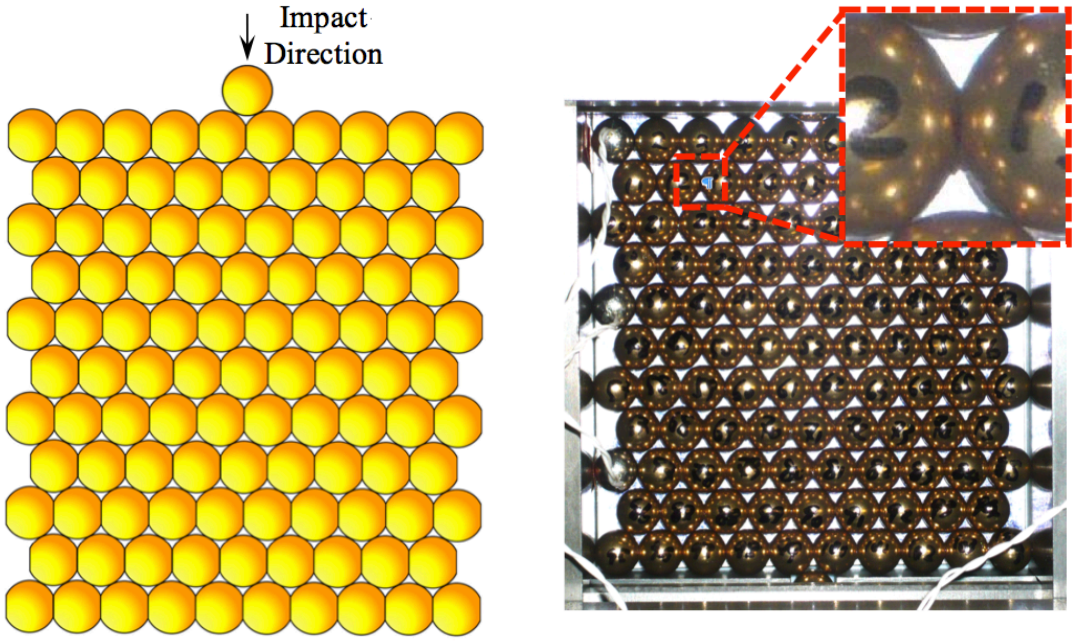

Figure B4.2: Schematic (left) and picture (right) of 2D granular packing with preconditioned beads. Preconditioning direction is horizontal.

Bead yield maps of the preconditioned bead packing at two different input loading levels are shown in Figure B4.5. For comparison, the yield map of the non-preconditioned bead packing case at the lower input loading level is also shown in Figure B4.5. It can be seen that the yielded contacts for the preconditioned bead packing are limited between the two 60 degree rows connecting those beads to the impact point. This is very different from the yielded contacts for a non-preconditioned bead packing, which is shows no preferred direction for occurrence of plasticity. ***Therefore, the 2D preconditioned bead packing can essentially be used to perform directional plasticity control.***

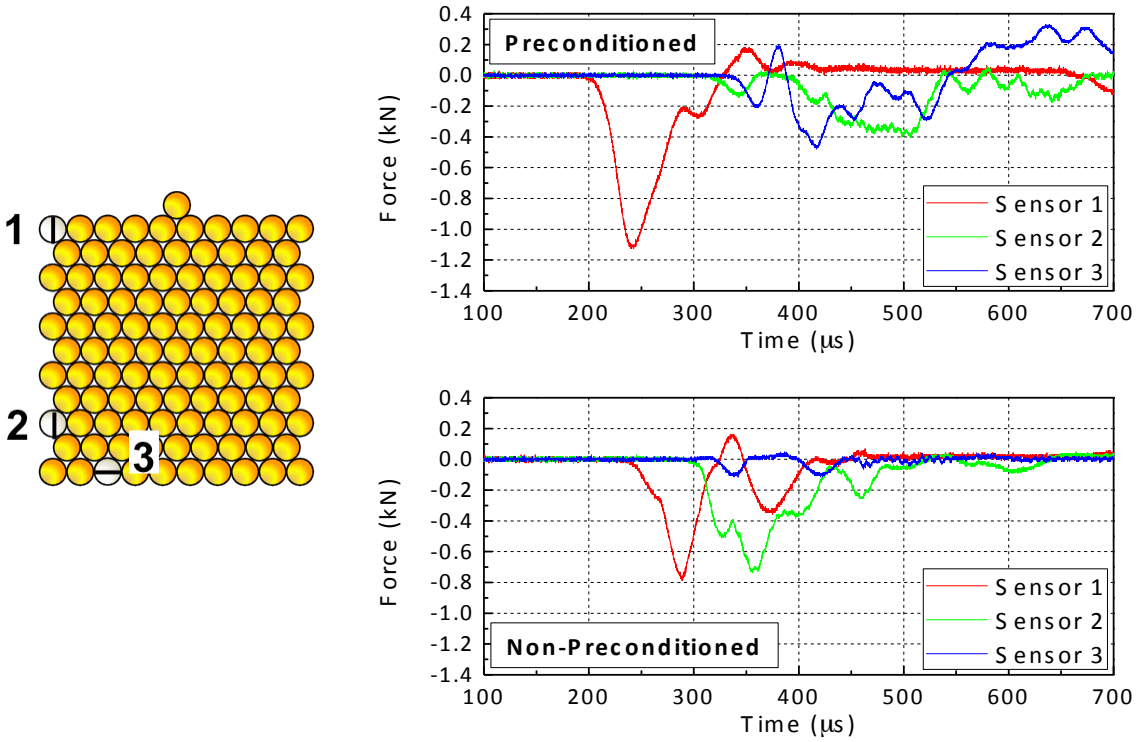

Figure B4.3: Wave profiles at three locations in a 2D horizontally preconditioned packing.

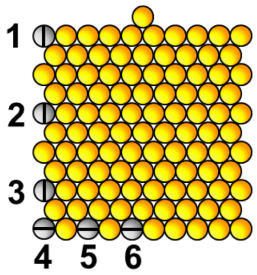

(a) Sensor locations

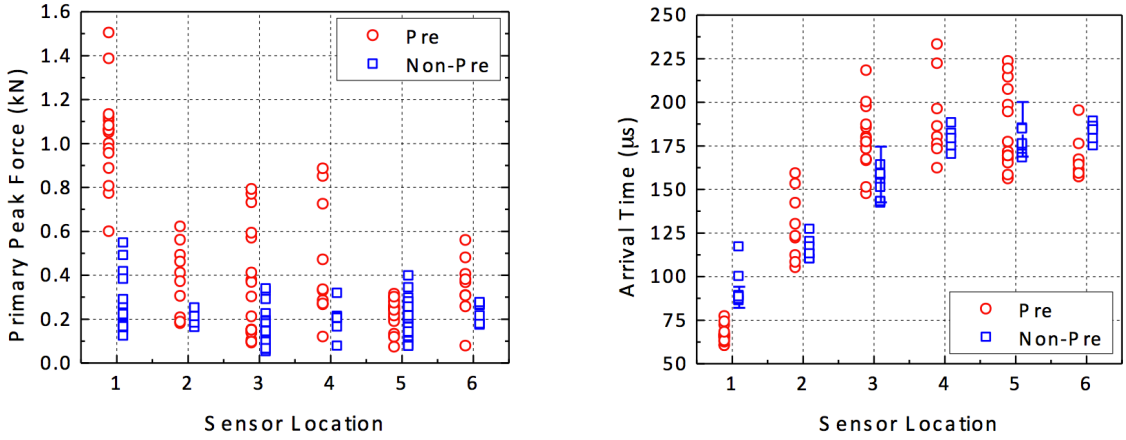

(b) Primary peak magnitude (c) Arrival time

Figure B4.4: Comparison of the primary peak pulse force magnitude and arrival time at six bead locations for preconditioned and non-preconditioned packings.

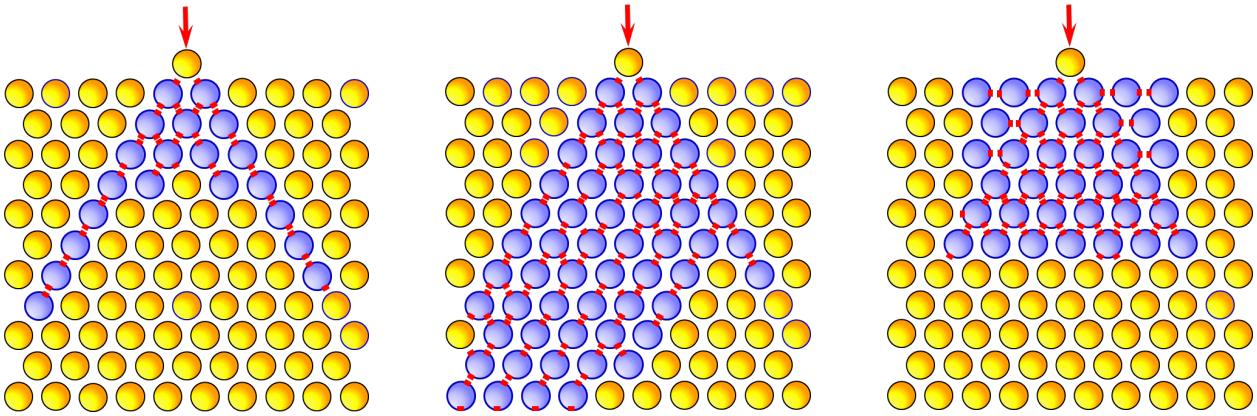

(a) Preconditioned, low input (~6 kN)

(b) Preconditioned, high input (~17 kN)

(c) Non-Preconditioned, low input (~10 kN)

Figure B4.5: Yield maps of preconditioned and non-preconditioned packing at different input loading level. Yellow: non-yielded bead; Blue: yielded beads; Red: yield location.

B5. 2D-plastic: Wave propagation in a 2D granular packing with intruders at optimized locations

In this part of out effort the research objectives were to (i) design and implement a self-standing 2D granular packing with intruders at optimized locations for certain force or energy metrics, (ii) experimentally obtain data for validation of numerical optimization scheme. The split Hopkinson pressure bar apparatus was used to impact the specimen to generate an elasto-plastic wave, as shown in Figure B5.1. A square packing with 11 (perpendicular to the impact direction) by 10 (parallel to the impact direction) rows of beads was used. The beads were made of brass alloy 260 (Young's modulus: 115 GPa; Yield strength: 550 MPa; Density: 8500 kg/m^3) with a diameter of 9.53 mm. The intruders occupying interstitial positions of the square lattice were cylinders made of stainless steel 302 and with a 3.95 mm diameter and 9.53 mm height, which can be fitted exactly into each space between four main beads, as shown in Figure B5.1.

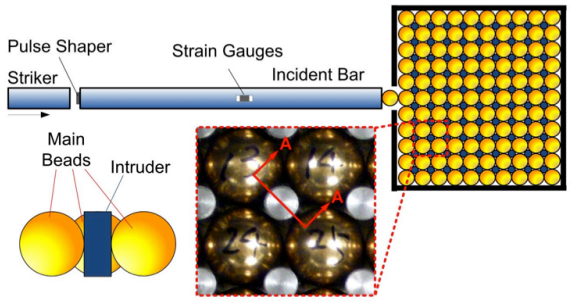

Figure B5.1: Experimental setup

Three optimized intruder layouts for maximizing maximum transmitted force over the region denote by a black line in Figure B5.2, but each with a restriction on the number of intruders used, have been numerically predicted. The corresponding experimental layouts are also shown in Figure B5.2. Here, the first layout from left is restricted to having 10 intruders, the second 30 intruders, and the third one 50 intruders. In addition, a square packing with intruders everywhere (total of 99 intruders) was also studied and this layout is shown in the fourth column in Figure B5.2. Three piezoelectric bead sensors were placed over the black line region on the right of each array to measure the normal contact forces between the sensor beads and the wall.

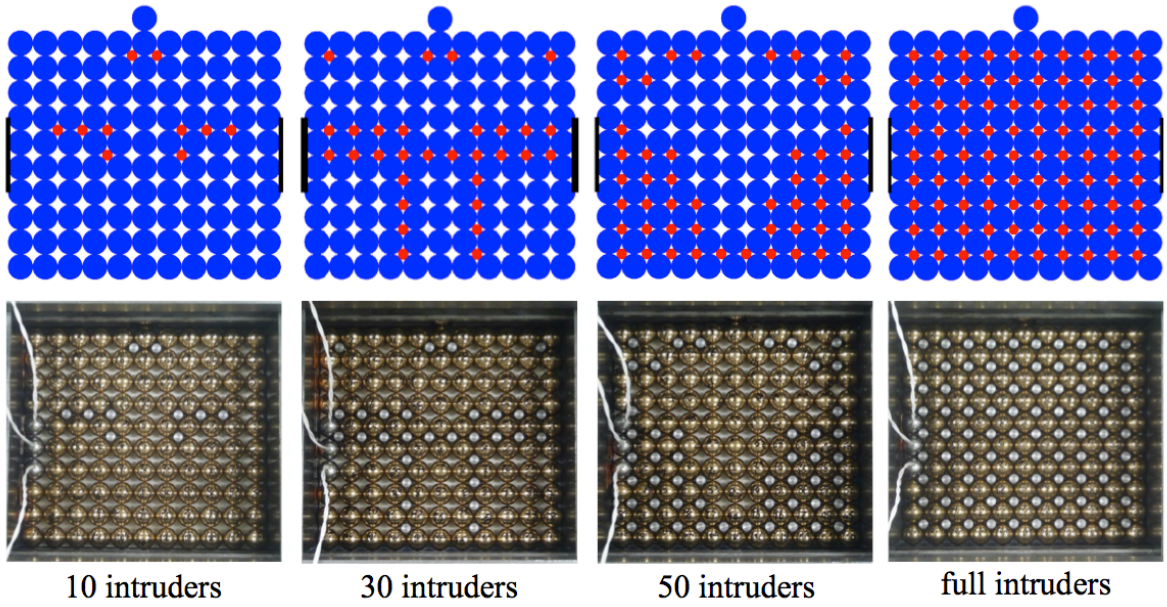

Figure B5.2: (Above) Optimized layouts for maximum side force with different intruder quantity restriction and (below) their corresponding experimental layouts.

The measured wave profiles at different sensors for different layouts are shown in Figure B5.3. The numerically predicted wave profiles are also shown here for comparison. It can be seen that the wave profiles for different layouts clearly show different arrival time and different peak value (primary peak) of the pulses. The trend of the arrival time and primary peak value from the experimental data roughly matches that from the numerical prediction for a perfect system. ***It clearly indicates that the numerical optimization algorithm in this study is robust for predicting the optimized layout.***

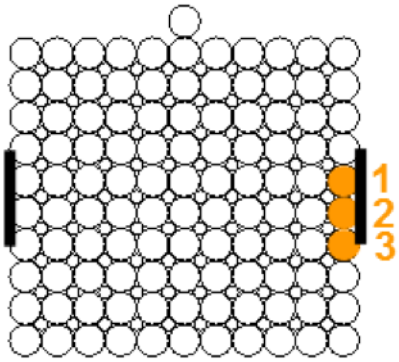

(a) Sensor locations

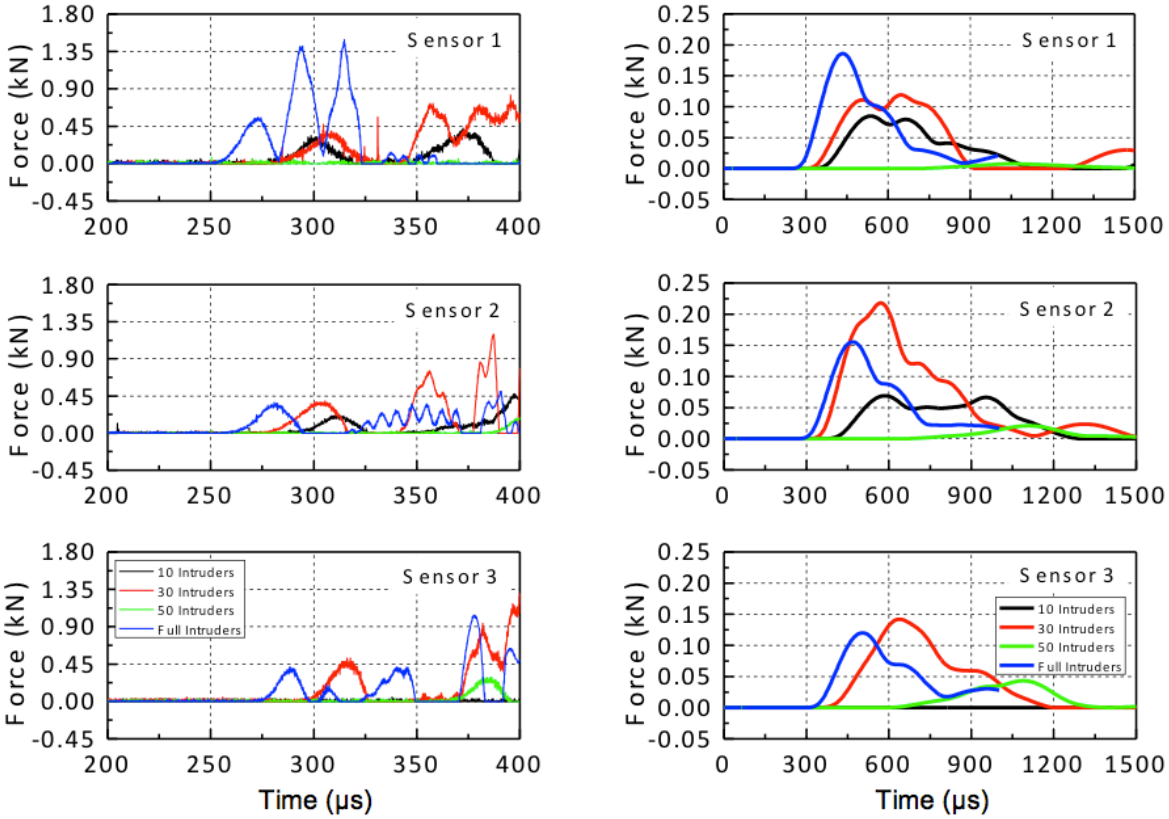

Experimental Numerical

(b) Wave profiles at different locations

Figure B5.3: Sensor location and measured wave profiles

Randomness cannot be avoided in these experiments and highly affects the results. It comes from many factors such as bead diameter tolerances, bead shape and misalignment of the beads in the packing. As a result, experimental and numerical studies on the effect of randomness were carried out in our study. Three methods were used to introduce experimental randomness: 1) use a new bead set; 2) use the old bead set but reassemble the entire packing; 3) use the old bead set and only reassemble the disturbed region. The experiment for each layout has been repeated at least five times. These experimental results have been summarized in Figures B5.4 and B5.5 for primary peak force value and arrival time as hollow circular points, respectively. The numerical results for a perfect system are also shown in these figures as the solid square points. It can clearly be seen that from the experimental results, randomness highly affects the primary peak force but less so the wave arrival time. The numerical prediction can capture the trend of the experimental results very well, while the absolute values from the numerical and experimental data are a bit off.

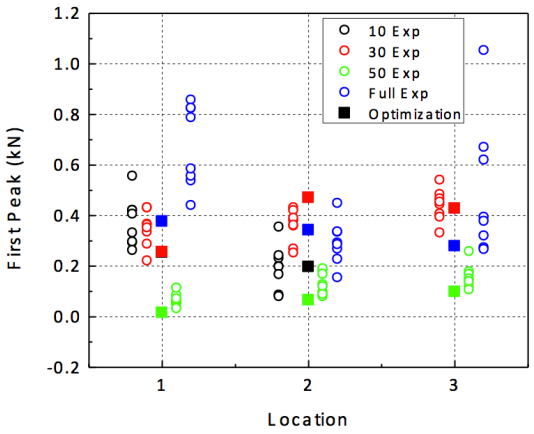

Figure B5.4: Primary peak force comparison

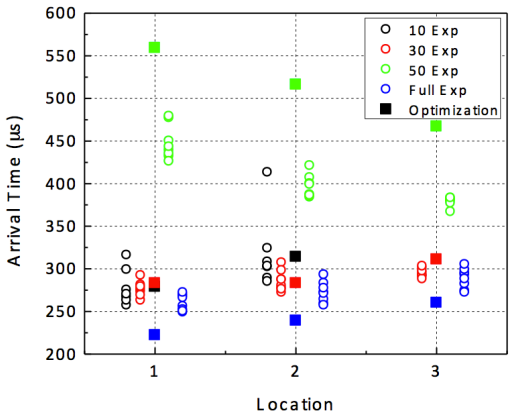

Figure B5.5: Wave arrival time comparison

B6. 2D-elastic and plastic: Continuum Microstructure Design

(a) Linear Elastic Response

The goal of the continuum material design is to optimize the microstructure of armor plates in a "functionally graded" way to control the flow of energy through the plate. This can be viewed as an ill-posed topology optimization problem wherein the goal is to optimally place different material constituents at each point in the body. To make this problem well-posed we use relaxation to expand the design space. In this way, rather than requiring each material point to consisting of one of the given material constituents, we allow each material point to be assigned a composite material that is fabricated from the given constituents. The elasticity tensor for the composite is obtained via homogenization.

Our study is limited to plane stress linear elastodynamic response of a two phase composite. The linear elastic and isotropic phases are combined to form a ranked laminate microstructure consisting of a stiff–heavy black phase and compliant–light gray phase, see Figure B6.1. At each material point in the body we optimize the relative density of the stiff phase ρ_i and laminate orientation φ_i. The rank 1 laminate is used as the matrix for the rank 2 laminate and so on. We limit ourselves to rank 3 laminates since they are able to represent any elasticity tensor (within the bounds of the two phases). We use analytical homogenization expressions to map the densities ρ_i and orientations φ_i to the elasticity tensor.

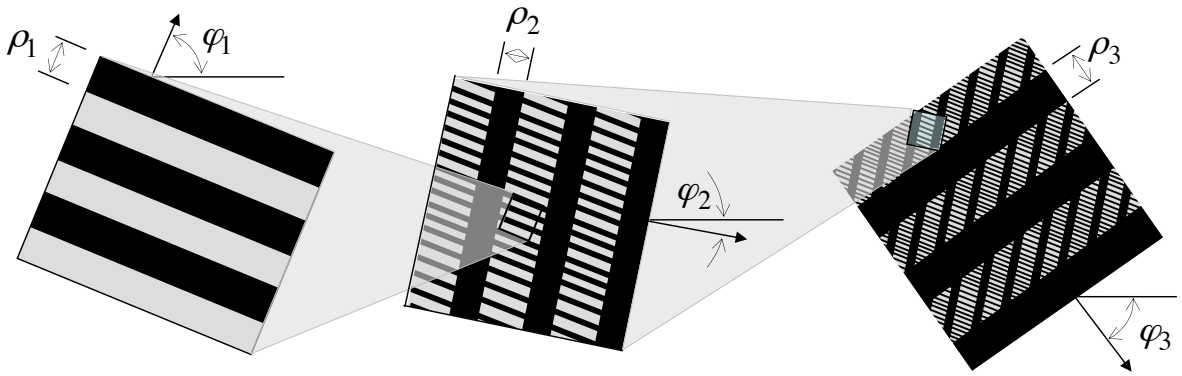

Figure B6.1: Ranked laminate.

As an example, we first consider the design of a plane stress linear elastic cantilever beam, see Figure B6.2. The beam is supported on the left boundary and subjected to the transverse tip load on its right boundary. The goal is to minimize the compliance, i.e., tip deflection, subject to a constraint on the mass. As expected, the beam's outer extents are comprised of the stiff-heavy phase, whereas the region near the neutral axis contains a mixture of the predominantly light-compliant phase.

The optimization problem is nonlinear even though the response of the beam is linear. To solve the optimization problem we use iterative nonlinear programming algorithms. The algorithm starts from an initial design, and at each iteration we compute the compliance and

mass as well as their gradients with respect to the relative density ρ_i and orientation φ_i fields. The gradients are evaluated analytically using the adjoint method.

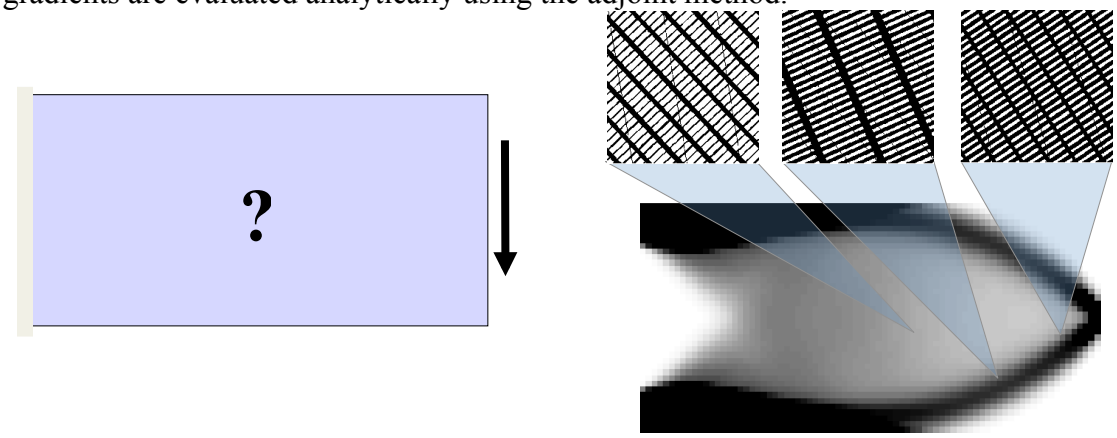

Figure B6.2: Cantilever beam optimization microstructure in which black and white represent the stiff–heavy and compliant–weak materials, respectively.

We use the finite element method to parameterize the density ρ_i and orientation φ_i fields as piecewise uniform over each finite element in the mesh. Using these ρ_i and φ_i element values we compute the element elasticity tensor and then perform a finite element analysis to compute the beam's compliance. The adjoint sensitivity analysis follows to compute the gradients of the compliance with respect to each of the ρ_i and φ_i element parameters. The gradient computation only requires a small percentage of the CPU versus the primal analysis itself. The optimization problem is large due to the large number of design parameters, i.e., 6 for each finite element in the mesh. Nonetheless, the problem is solved efficiently due to the use of gradient based optimization algorithms and highly efficient sensitivity analyses.

In our other applications we consider the dynamic response of a plane-stress plate that is subjected to an impact load. The goal in these optimizations is to direct the total energy, i.e., the kinetic plus strain energy, either towards or away from given locations in the plate. For example, as depicted in Figure B6.3 we impact the top of the plate and focus energy towards the bottom center of the plate by optimally designing the microstructure throughout the plate.

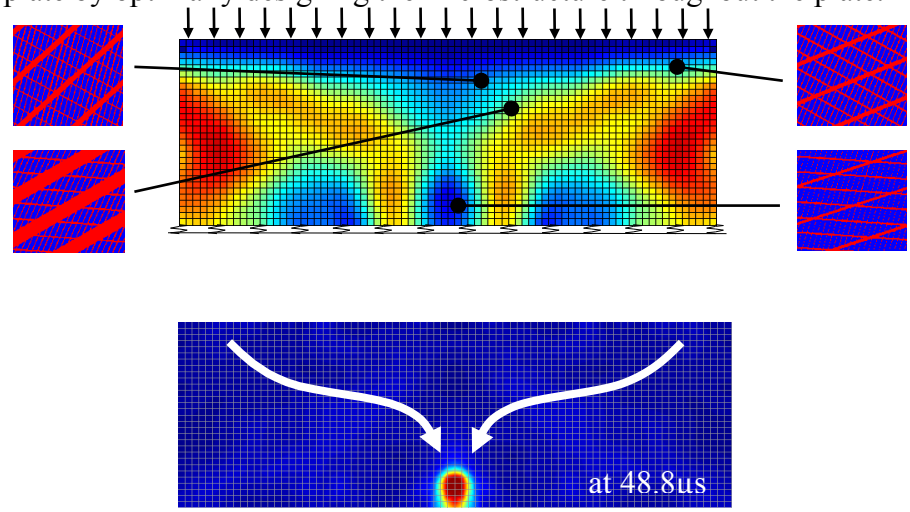

Figure B6.3: Optimized plate for energy focusing. Optimized microstructure in which red and blue represent the stiff–heavy and compliant–weak materials, respectively (top) and energy after 48.8 μs (bottom) where blue to red represents little to much energy.

The parameterization for this example by the finite element method is repeated as described above, here however the analyses are dynamic. The transient nature of the simulation complicates our adjoint sensitivity analysis. Specifically, the primal problem must be completed and trajectory saved before the sensitivity analysis begins. This presents implementation issues which we resolve using a distributed parallel computing environment. ***To our knowledge, this is the first use of topology optimizations for dynamic response.***

(b) Nonlinear Elastic Response

The above linear elastic designs are promising as they demonstrated the feasibility of solving topology optimization problems for dynamic response. However, we expect armor plates to operate in nonlinear regimes. Hence we extend our scope to the realm of finite deformation hyperelasticity. This extension comes with two primary challenges, 1) the analytical homogenization expressions are not available and 2) the primal analysis is nonlinear.

Because the analytical homogenization expressions are not available we resort to numerical methods. Previously, at each material point the composite material was described by a unit cell consisting of a ranked laminate. Now each composite material point is described by a unit cell that contains an arbitrary distribution of stiff–heavy and compliant–weak material phases, see Figure B6.4. To evaluate the composite unit cell's homogenized properties we use finite element analysis. Each unit cell is meshed and each cell element is assigned a single phase, i.e., stiff–heavy or compliant–weak. Given a macroscopic strain, the homogenization equations are solved over the unit cell via finite element simulation to evaluate its homogenized stress and incremental elasticity tensors. The equations are nonlinear and solved via Newton-Raphson iteration.

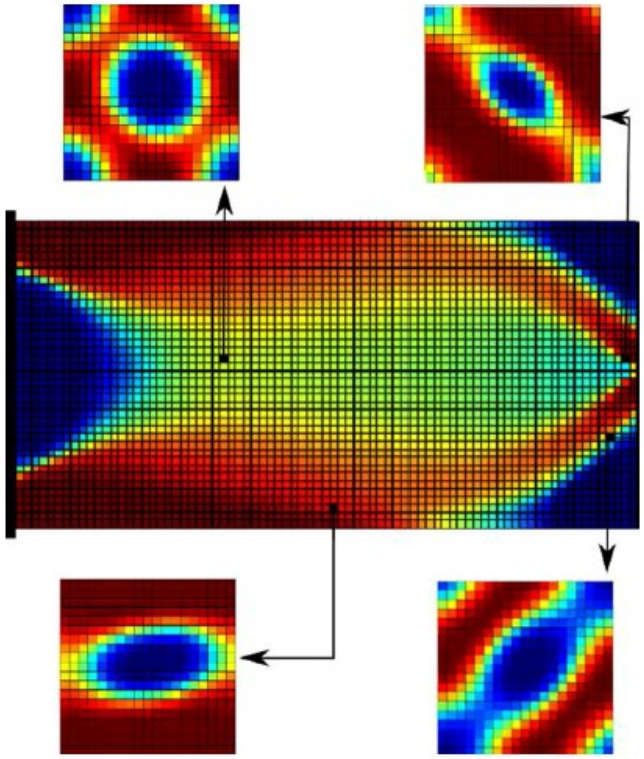

Figure B6.4: Optimized nonlinear elastic cantilever beam in which red and blue represent the stiff–heavy and compliant–weak materials, respectively.

Now that we can evaluate the homogenized stress and incremental elasticity tensors we can go about solving the governing equation throughout the structure. We first consider the static case and thus the governing equation is that of equilibrium. This equilibrium equation is nonlinear and solved as above by combining the finite element method with the Newton-Raphson iterative solver. At each iteration we evaluate the strain field and use that strain to evaluate the homogenized stress and incremental elasticity tensors. This multiscale analysis is efficiently solved by computing the algorithmic consistent tangent matrix.

In the linear case the optimization control is the density ρ_i and orientation φ_i fields. Here the control is the indicator field over the unit cell. At each point in the unit cell the indicator value tells us which material is present, i.e., the stiff–heavy or compliant–weak. This ensuing design problem of optimizing the indicator field over the unit cell for each material point in our structure has two issues 1) it is ill-posed and 2) it is nonconvex which precludes the use of efficient nonlinear programming algorithms. To make the problem well-posed we use restriction whereby we no longer allow for an arbitrary distribution of the material phases within the unit cell. Rather we restrict the minimum length scale to disallow chattering designs wherein an infinite number of infinitesimally small regions of distinct material phases appear in the unit cell. To make the problem convex we replace the indicator field with a volume fraction field which specifies the percentage of the stiff–heavy versus compliant–weak phase at each point in the unit cell. This means mixtures of materials are present which is not physically possible. However, we penalize mixtures in our optimization and thereby our designs only have small interphase regions where mixtures exist.

As seen in Figure B6.4, the volume fraction field is parameterized to be piecewise uniform over each of the finite elements in each of the unit cells. Thusly we have literally thousands of design parameters, i.e., one for each finite element in the unit cell times the number of finite elements in the macroscopic, i.e. structural, mesh. This large–scale optimization problem is again efficiently solved by combining nonlinear programming algorithms with efficient adjoint sensitivity analysis. Indeed, although the sensitivity requires the solution to an adjoint problem, the adjoint problem is linear and can be efficiently solved by using the decomposed tangent matrix from the primal analysis. In this way, the sensitivity analysis is virtually cost free when compared to the cost of the primal analysis.

We now consider the nonlinear elastic counterparts to the previously discussed elastic design problems. Here the nonlinear Neo-Hookean isotropic constituents consist of a stiff–heavy (red) phase and a compliant–light (blue) phase. Figure B6.4 illustrates the optimized beam design wherein we again see predominantly stiff–heavy phase along the beam's outer extents and compliant–light phase along its neutral axis. Figure B6.5 illustrates the dynamic counterpart to the design that appears in Figure B6.3. There is a noticeable difference between the linear and nonlinear designs.

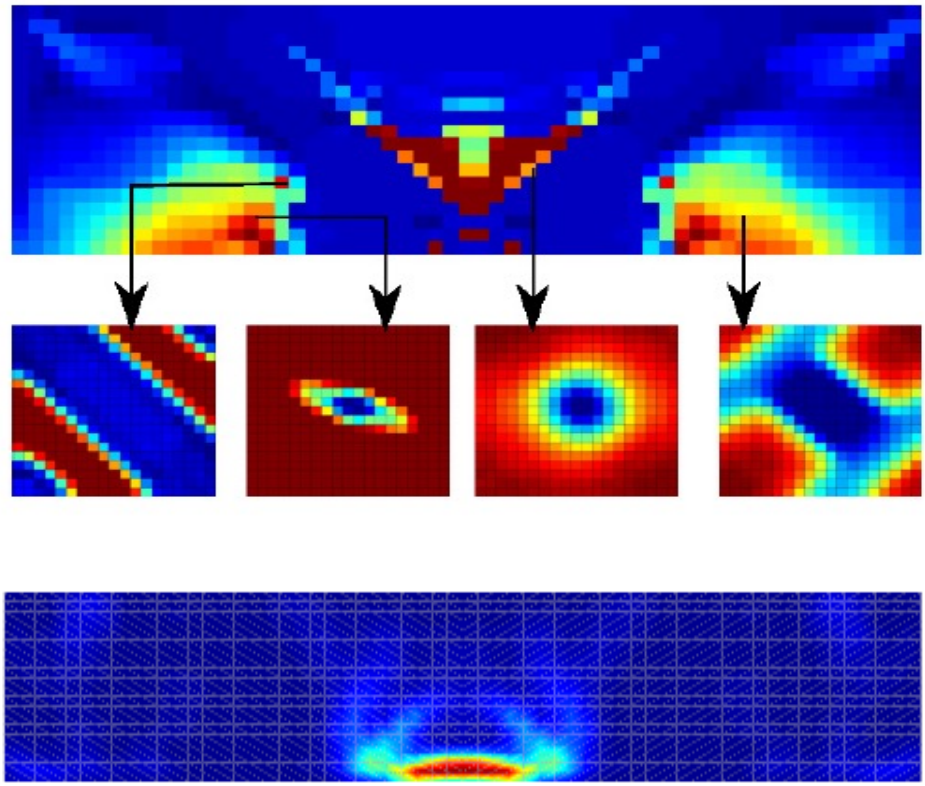

Figure B6.5: Optimized nonlinear elastic plate for energy focusing. Optimized microstructure in which red and blue represent the stiff—heavy and compliant—weak materials, respectively (top) and energy after 40 μs (bottom) where blue to red represents little to much energy.

(c) Nonlinear Elasto-plastic Response

In the elastic studies the macrostructure is a composite body wherein each material point is described by a unit cell that contains a distribution of the two material phases. Unfortunately, the procedure for manufacturing such functionally graded bodies is not straight forward since it would require us to adjoin neighboring unit cells. For example, it may require us to join stiff-heavy phases to compliant–light phases which would obviously affect the material response in the local unit cell ensemble. To remedy this problem, we take a different approach wherein we specify the material phase that is present at each material point in the macro structure. In so doing, we are no longer designing a composite body, rather we are designing a heterogeneous body where each material point is one of the two phases. This problem is akin to the unit cell design problem we discussed in the guise of nonlinear elasticity. As such, we use restriction to enforce a minimum length scale and we replace the material indicator field with a volume fraction field to convexify the design space. However, unlike the nonlinear case, no penalization is required to achieve designs in which the material distribution is solely one phase or the other, with the exception of the small interphase regions where mixtures exist.

To make our research more relevant we incorporated elasto-plastic behavior into our designs. So now the stiff–heavy and compliant–weak phases that were previously described by Neo-Hookean isotropic material models are replaced by strong–stiff–heavy and weak–

compliant–light phases that are described by small strain von Mises material models. This material model complicates the simulation and sensitivity analysis since we now have to solve the material evolution equation which governs the associated state-variable. Further enhancements were made by considering three-dimensional response. Figure B6.6 illustrates our design problem in which the plate is subjected to an impulse load over the concentrated center region. The goal of the optimization is to minimize the energy in the four rectangular target regions along the plates outer boundary. As expected, the strong–stiff–heavy material is located under in the load application and target regions, however aside from that, the material distribution is not intuitive.

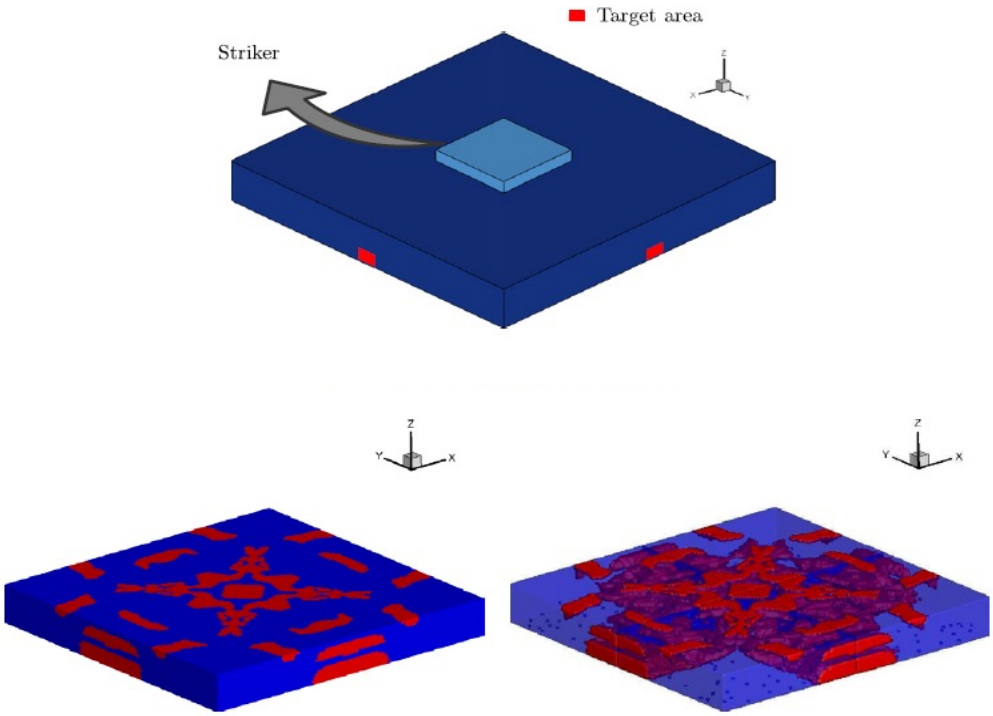

Figure B6.6: Three dimensional plate with striker location and target areas (top), . Optimized design in which red and blue represent the strong–stiff–heavy and weak–compliant–light materials, respectively (bottom left) and associated translucent view (bottom right).

B7. Other efforts on material fabrication

Objectives

(a) Design and fabrication of model systems for the experimental support and verification of theoretical models developed by other members of the MURI group.
(b) Synthesis of ceramic beads of any composition and size for use in experimental validation
(c) Determination of static, as well as dynamic properties of ceramics and ceramic composites under ballistic conditions
(d) Investigation of what conditions are necessary for the nucleation of phase transformations in ceramics under ballistic impact
(e) Design and synthesis of laminated ceramic composites exhibiting stress wave mitigating effects
(f) Design of real ceramic composite materials employing the concepts developed thus far

Approach

The Kriven Group approach was to fabricate ceramic beads of any chemistry by one of two processes. The first is a sol gel droplet method for beads that are less than 5 mm in diameter. The second is a vibratory approach for beads that are greater than 5 mm. The first method has been developed in collaboration with Prof. Bumrae Cho who was a visiting professor from Keimyung University, South Korea. A manuscript describing this method published in the Journal of the American Ceramic Society. The second method has also successfully been developed within our laboratories, and a second manuscript describing this process was published in the Journal of the European Ceramic Society. This work was carried out by the Ph.D. student, Christian Espinoza.

Once the beads have been fabricated they needed to be tested under dynamic conditions. This is done in collaboration with the Vakakis Group for beads suspended from a vertical thread, and beads in a row for the Split Hopkinson Bar test. The beads are tested in a hollow tube and when dispersed in a carbon fiber reinforced geopolymer matrix. To this end, the static properties (compressive and bend strength, as well as toughness) geopolymer matrix itself need to be measured and calibrated. The geopolymer matrix offers a quick method for fabricating bead arrays in various geometrical configurations in a ceramic matrix. To date, we have determined the optimum synthesis conditions and that the effect of the matrix on the linear bead array can be made identical to whether the matrix is present or absent. A collaboration on more advanced and systematic mechanical evaluation such as Poisson's ratio and Weibull modulus was completed with Prof. Eldon Case at the University of Michigan in Ann Arbor. This work was carried out by Shinho Cho.

Tape cast laminates of dense alumina (Al_2O_3) or mullite ($3Al_2O_3 \cdot 2SiO_2$) ceramics separated by weak, porous ceramics are being fabricated, using porous alumina or porous aluminum phosphate ($AlPO_4$). Not only are the laminates stacked in parallel 0° orientation, they are also being stacked in oblique orientations (e.g. ± 45° and 90° orientations). Other angular orientations are being made as a result of collaboration with the Tortorelli Group. Evaluation of the dynamic properties of such laminated composites as a function of laminate inclination are being carried out in the Brazilian disc mode, in collaboration with the Lambros Group. Discs of laminated composites were cut and placed at various inclinations between vertical and horizontal, in a Split Hopkinson Bar apparatus and their mechanical performance was analyzed. This work was done by Dr. Pathikumar Sellapan and Christian Espinoza.

References

Awasthi, A., Smith, K., Geubelle, P. H. and Lambros, J. (2012) "Propagation of solitary waves in 2D granular media: a numerical study." *Mechanics of Materials*, **54**, 100-112.

Awasthi, A. P., Wang, Z., Broadhurst, N. R., and Geubelle, P. H. (2015) "Impact response of granular layers." *Granular Matter*, **17**, 21-31. DOI: 10.1007/s10035-015-0547-3.

Boechler N., Theocharis G. and Daraio C. (2011), "Bifurcation-based acoustic switching and rectification", Nature materials, Vol. 10(9), pp. 665–668.

Fogarassy, E. and D. Geohegan (2012), Laser Ablation, Elsevier Science.

Leonard, A., Daraio, C., Awasthi, A. and Geubelle, P. H. (2012) "Effect of weak disorder on stress-wave anisotropy in centered square nonlinear granular crystals." *Physical Review E*, **86**, 031305-1-10. DOI: 10.1103/PhysRevE.86.031305.

Manjunath, M., Awasthi, A. P. and Geubelle, P. H. (2012) "Wave propagation in random granular chains." *Physical Review E*, **86**, 031308. DOI: 10.1103/PhysRevE.85.031308.

Manjunath, M., Awasthi, A. P., and Geubelle, P. H. (2014a) "Wave propagation in 2D random granular media." *Physica D: Nonlinear Phenomena*, **266**, 42-48. DOI: http://dx.doi.org/10.1016/j.physd.2013.10.004.

Manjunath, M., Awasthi, A. P., and Geubelle, P. H. (2014b) "Plane wave propagation in 2D and 3D mono-disperse periodic granular media." *Granular Matter*, **16:1**, 141-150. DOI:10.1007/s10035-013-0475-z.

Manjunath, M., Awasthi, A. P., and Geubelle, P. H. (2014c) "A family of plane solitary waves in dimer granular crystals." *Physical Review E*, **90**, 032209. DOI:10.1103/Physreve.90.032209.

Nesterenko V.F. (1984), "Propagation of nonlinear compression pulses in granular media" Journal of Applied Mechanics and Technical Physics, pp. 733-743.

Nesterenko V.F. (2001), Dynamics of Heterogeneous Materials, Springer-Verlag, 522 pages, New York.

Pal, R. K., Awasthi, A, P. and Geubelle, P. H. (2014a) "Characterization of wave propagation in elastic and elasto-plastic granular chains." *Physical Review E*, **89**, 012204-1 to 10. DOI: 10.1103/PhysRevE.89.012204.

Pal, R. K. and Geubelle, P. H. (2014a) "Impact response of elasto-plastic granular and continuum systems: A comparative study." *Mechanics of Materials*, **73**, 38-50. DOI: 10.1016/j.mechmat.2014.02.006.

Pal, R. K., Morton, J., Wang, E., Lambros, J., and Geubelle, P. H. (2014b) "Impact response of elasto-plastic granular chains containing an intruder particle." *Journal of Applied Mechanics*, **82:1**, 011002. DOI: 10.1115/1.4028959.

Pal, R. K., and Geubelle, P. H. (2014b) "Wave tailoring by precompression in confined granular systems." *Physical Review E*, **90**, 042204. DOI: Artn 042204 DOI:10.1103/Physreve.90.042204.

Spadoni A. and Daraio C. (2010), "Generation and control of sound bullets with a nonlinear acoustic lens", Proceedings of the National Academy of Sciences, Vol. 107(16), pp. 7230–7234.

Wang, E., Manjunath, M., Awasthi, A. P., Pal, R. K., Geubelle, P. H. and Lambros, J. (2014) "High-amplitude elastic solitary wave propagation in 1-D granular chains with preconditioned beads: experiments and theoretical analysis." *Journal of the Mechanics and Physics of Solids*, **72**, 161-173. DOI: 10.1016/j.jmps.2014.08.002.